nature protocols

https://doi.org/10.1038/s41596-023-00941-5

Protocol

Check for updates

Spatial analysis of tissue immunity and vascularity by light sheet fluorescence microscopy

Duo Zhang[1], Abigail H. Cleveland[1], Elisavet Krimitza[1], Katherine Han[1], Chenlong Yi[2], Andrea L. Stout[3], Wei Zou[1], Jay F. Dorsey[1], Yanqing Gong[2] ✉ & Yi Fan[1] ✉

Abstract

The pathogenesis of cancer and cardiovascular diseases is subjected to spatiotemporal regulation by the tissue microenvironment. Multiplex visualization of the microenvironmental components, including immune cells, vasculature and tissue hypoxia, provides critical information underlying the disease progression and therapy resistance, which is often limited by imaging depth and resolution in large-volume tissues. To this end, light sheet fluorescence microscopy, following tissue clarification and immunostaining, may generate three-dimensional high-resolution images at a whole-organ level. Here we provide a detailed description of light sheet fluorescence microscopy imaging analysis of immune cell composition, vascularization, tissue perfusion and hypoxia in mouse normal brains and hearts, as well as brain tumors. We describe a procedure for visualizing tissue vascularization, perfusion and hypoxia with a transgenic vascular labeling system. We provide the procedures for tissue collection, tissue semi-clearing and immunostaining. We further describe standard methods for analyzing tissue immunity and vascularity. We anticipate that this method will facilitate the spatial illustration of structure and function of the tissue microenvironmental components in cancer and cardiovascular diseases. The procedure requires 1–2 weeks and can be performed by users with expertise in general molecular biology.

Key points

- The protocol covers tissue preparation, polymerization, tissue semi-clearing, immunostaining, refractive index matching and mounting, imaging, and data processing and analysis.
- The mild processing of samples ensures structural and molecular stability, preserving most of the proteins of interest for antibody-based immunostaining.

Key references

Wang, Q. et al. *Nat. Commun.* **9**, 559 (2018): https://doi.org/10.1038/s41467-018-03050-0

Ma, W. et al. *Nat. Cancer* **2**, 83–97 (2021): https://doi.org/10.1038/s43018-020-00147-8

Huang, M. et al. *Nat. Cardiovasc. Res.* **1**, 372–388 (2022): https://doi.org/10.1038/s44161-022-00047-3

Zhang, D. et al. *Cell Metab.* **35**, 517–534 (2023): https://doi.org/10.1016/j.cmet.2023.01.010

[1]Department of Radiation Oncology, University of Pennsylvania, Philadelphia, PA, USA. [2]Department of Medicine, University of Pennsylvania, Philadelphia, PA, USA. [3]Department of Cell and Developmental Biology, University of Pennsylvania, Philadelphia, PA, USA. ✉e-mail: gongy@pennmedicine.upenn.edu; fanyi@upenn.edu

Introduction

Spatiotemporal regulations of tissue microenvironmental components, including vasculature and immune cells, play a crucial role in disease progression and therapeutic responses[1–3]. Aberrant vasculature creates an immunosuppressive and inaccessible microenvironment. This induces the exclusion of T cells and therapeutic components[4–8] and impedes the reperfusion of the infarcted area in the context of cardiac repair[9–11]. Imaging vascularity, immune components and other elements in the tissue microenvironment are essential for understanding the pathogenic mechanisms in cancer and cardiovascular diseases (CVD) and for testing novel therapeutic strategies.

Traditional thin tissue slides of 5–100 µm used in epifluorescence or confocal microscopy provide limited information about the tissue microenvironment, making it difficult to reliably analyze the vascular structure and perfusion dynamics, immune cell composition and functions, and the interactions between microenvironmental components[12]. Whole-organ-level three-dimensional (3D) fluorescent imaging techniques, such as light sheet fluorescence microscopy (LSFM)[13], coupled with advanced tissue-clearing techniques, such as DISCO[14–18], CUBIC[19–23], Sca*l*e[24,25] and CLARITY[26,27], have been developed to overcome the limitations of imaging depth and resolution. However, current innovations in 3D fluorescent imaging protocols and pipelines mainly require lengthy processing efforts and highly specialized equipment and reagents[28]. Moreover, most existing protocols employ reagents that may compromise tissue integrity and disrupt endogenously expressed reporter fluorescent proteins[29]. These labor-intensive procedures and high initiation hurdles therefore make 3D fluorescent microscopy challenging to be implemented for standard biology laboratories that are often not specialized in microscopy or bioengineering. To address these issues, we provide an optimized protocol that adopts concise hydrogel-based tissue clearing and LSFM pipelines to allow high reproducibility and low-cost analysis of tissue samples from mouse brain tumor[7,8] and myocardial infarction (MI)[11] models. The streamlined and standardized processes for semi-clearing and staining enable efficient light transmittance throughout the tissues. Importantly, this protocol prioritizes the preservation of endogenous fluorescent reporters and immune antigens. In addition, we incorporated a combination of genetic endothelial lineage tracing, lectin perfusion and hypoxia probing to determine vascular structure and function. We also employed a genetic fluorescent protein labeling system for imaging chimeric antigen receptor (CAR) T cell infiltration and presence[7]. We expect that this approach will facilitate tissue microenvironment phenotyping research in the fields of cancer, cardiovascular biology, immunotherapy and drug delivery for a biomedical laboratory equipped with routine histology technology.

Development of the protocol

Initially, the limited amount of information obtained through traditional microscopy methods prompted the development of the protocol and adoption of 3D-imaging methodology. In the rapidly advancing field of high-dimensional imaging, various methodologies have emerged, offering distinct advantages for specific applications. Laser-scanning confocal microscopy provides high-resolution and high-contrast images but is limited by potential photodamage and imaging depth. Spinning disk confocal microscopy generates fast images of live samples but is restricted by low-imaging resolution and depth. Multiphoton microscopy excels in live tissue imaging with deeper-imaging capabilities and less phototoxicity; however, its acquisition speed can be slower due to the scanning mechanism. Super-resolution microscopy techniques, such as stimulated emission depletion and photo-activated localization microscopy/stochastic optical reconstruction microscopy, extends resolution limits to the molecular level at the cost of complexity and computational resources. In contrast, LSFM presents an advantageous balance of high-resolution imaging, speed, minimal phototoxicity and the capacity to image large samples, making it an ideal technique for tissue to organ-level 3D fluorescent imaging. LSFM generates thin slices of light that illuminate a specific plane of the sample. The fluorescence emitted from this plane is picked by an objective lens and then

captured by a camera oriented perpendicularly to the light sheet. Imaging time intervals are shorter than other light microscopy techniques and the out-of-focus light impact is less. LSFM images compiled in *Z*-stacks contain exponentially more information with high resolution at an organ level, compared with planar images and common histology analysis methods, such as counting high-intensity spots or measuring surface area. There are potentially biases introduced by two-dimensional tissue slides when analyzing characteristics such as vascularization and tissue perfusion, in which 3D visualization is required for accurate assessment of volumetric features such as vessel volume, branching and surface area. Similarly, LSFM will contribute to better understanding of spatial regulation of T cell immunity in tissues.

To precisely analyze tissue vascularity, we chose a *Cdh5–Cre*^{ERT2}*;Rosa–LSL–tdTomato* endothelial lineage tracing system in mice[30]. Staining analysis based on endothelial markers does not allow to accurately visualize whole vasculature, because endothelial cells (ECs) exhibit robust cell plasticity in cancer and CVD (cardiovascular) conditions. The endothelial to mesenchymal transition may lead to of expression loss of endothelial markers such as VE-cadherin or CD31 in ECs[31,32]. Furthermore, we have utilized additional approaches to further determine vascular function, by intravenously injecting fluorophore-conjugated lectin and hypoxyprobe to image tissue perfusion and hypoxia[8,11].

To preserve tissue integrity and protein content, we adopted a mild fixation and semi-clearing pipeline that uses a CLARITY/PACT tissue clearing and staining protocol[27], over other workflows that involve solvent-based dehydration or solvent-based refractive index (RI) matching. This modified tissue semi-clearing protocol, coupled with LSFM, has allowed us to visualize tdTomato$^+$ vasculature along with regions of hypoxia in tumors and with lectin perfusion in ischemic hearts in *Cdh5–Cre*^{ERT2}*;Rosa–LSL–tdTomato* mice. Importantly, this optimized protocol helps preserve tissue antigen and structure while being permissive of immunofluorescence staining, by which we have imaged infiltrating CD3$^+$ T cells and tdTomato$^+$ vasculature in mouse brain tumors[7]. Furthermore, based on our recently developed CAR T cell tracing system[7], we optimized and streamlined our protocol to be compatible with immunofluorescence staining with antibodies against additional immune cell function makers, which can be used to study the spatial dynamics and distribution of CAR T cells and other immune cells within the tumor. This advancement offers a new tool to provide spatial resolution of tissue vascularity and immunity, contributing to the understanding of microenvironment-dependent regulatory mechanisms for disease development and therapy resistance.

Advantage of the protocol and comparison with other methods

One of the main advantages of the developed protocol is the usage of genetic labeling systems to image vascular ECs and immune cells in pathological settings. For example, the *Cdh5–Cre*^{ERT2}*;Rosa–LSL–tdTomato* system ensures accurate imaging of the vasculature in disease contexts. Expression of fluorescent reporter gene (mTagBFP2) allows T cell visualization in the tissues. Notably, *Cdh5–Cre*^{ERT2} has a well-established rigid specificity to vascular ECs, compared with other promoters/enhancers, such as Tie2–Cre that can also be expressed in non-EC myeloid cells[33,34]. With a brightness triple that of enhanced GFP, tdTomato is one of the brightest fluorescent proteins in the current genetic reporter toolbox and provides robust EC-labeling in suboptimal conditioned samples with pigmentation or blood retention, which can be commonly found in tumor tissue[35,36].

Another notable advantage is the combined use of lectin and hypoxia probe for a comprehensive analysis of vessel function and structure. This allows for a better understanding of the vascular system in various tissues and disease conditions, as it enables researchers to study not only the morphology of blood vessels but also their functional aspects such as perfusion and oxygenation. Such a comprehensive approach is essential for understanding the complex interplay between the microenvironment and the vasculature in diseases such as cancer and cardiovascular disorders.

Furthermore, the protocol employs mild processing of samples and aims for maximum structural and molecular stability, preserving most of the protein of interest for antibody-based

immunostaining. This approach ensures that the samples remain stable for months or even years, allowing for long-term storage and analysis. In contrast to workflows that incorporates solvent-based delipidation using methanol, ethanol or tetrahydrofuran, dehydration of tissue can cause conformational change of fluorescent proteins, leading to rapid quenching within hours or days[14,37,38]. This protocol is particularly advantageous in cases where researchers need to image fluorescent proteins or perform retrospective analyses and compare results from different experiments conducted at different timepoints.

In addition, incorporation of CLARITY-based hydrogel embedding maximizes biomolecule retention, allowing the staining and imaging of markers in rare cell populations, such as tumor-infiltrating T cells or CAR T cells, In the rapidly advancing field of high-dimensional imaging, various methodologies have emerged, offering distinct advantages for specific applications. Laser-scanning confocal microscopy provides high-resolution and high-contrast images but is limited by potential photodamage and imaging depth. Spinning disk confocal microscopy generates fast images of live samples but is restricted by low-imaging resolution and depth. Multiphoton microscopy excels in live tissue imaging with deeper-imaging capabilities and less phototoxicity; however, its acquisition speed can be slower due to the scanning mechanism. Super-resolution microscopy techniques, such as stimulated emission depletion and photo-activated localization microscopy/stochastic optical reconstruction microscopy, extend resolution limits to the molecular level at the cost of complexity and computational resources. In contrast, LSFM presents an advantageous balance of high-resolution imaging, speed, minimal phototoxicity and the capacity to image large samples, making it an ideal technique for tissue to organ-level 3D fluorescent imaging. LSFM generates thin slices of light that illuminate a specific plane of the sample. The fluorescence emitted from this plane is then captured by a camera oriented perpendicularly to the light sheet. By moving the light sheet across the sample, a series of images are captured, which can be compiled to form a comprehensive 3D image.

Limitations

While the protocol has many advantages, it also comes with some limitations. For instance, it lacks decolorization and decalcification steps that are crucial to optical clarity. Consequently, imaging bone tissue, skin tissue with pigmentation or colored tumors such as melanoma becomes difficult. In addition, without the bleaching process, the red color of internal bleeding spots and necrotic cores of tumors may remain, which can potentially affect the lateral penetration depth of the image and limit the overall imaging quality. We circumvented this problem by limiting the size of sample and region of interest (ROI) in exchange for better transmittance along the *z* axis. For larger ROIs in samples with similar issues, sample processing and imaging methods may need to be modified.

The use of tdTomato as a fluorescent reporter may bring some challenges. Although it has high intensity, tdTomato has a wide emission wavelength that overlaps with other fluorescence channels, complicating the analysis of multiple signals in the same sample. Researchers must, therefore, be careful when choosing fluorophores, to minimize spectral overlap and potential interference. An alternative option could be enhanced GFP that has a narrower excitation/emission spectrum.

Lastly, Imaris, the commercial software used for 3D imaging deconvolution and analysis, can be costly. This may limit the accessibility of the protocol to researchers with limited funding or resources. Alternatively, it is important to consider other open-source software options or develop cost-effective solutions.

Experimental design

The experimental design of this study involves several crucial steps including sample preparation (Steps 1–9), hydrogel polymerization (Steps 10–14), tissue clearing (Steps 15–17), immunostaining (Steps 18–23), RI matching and mounting (Steps 24–32), imaging (Steps 33–40), and data processing and analysis (Steps 41–50) (Fig. 1). These steps are necessary to achieve accurate and reliable results in the spatial analysis of tissue immunity and vascularity using LSFM.

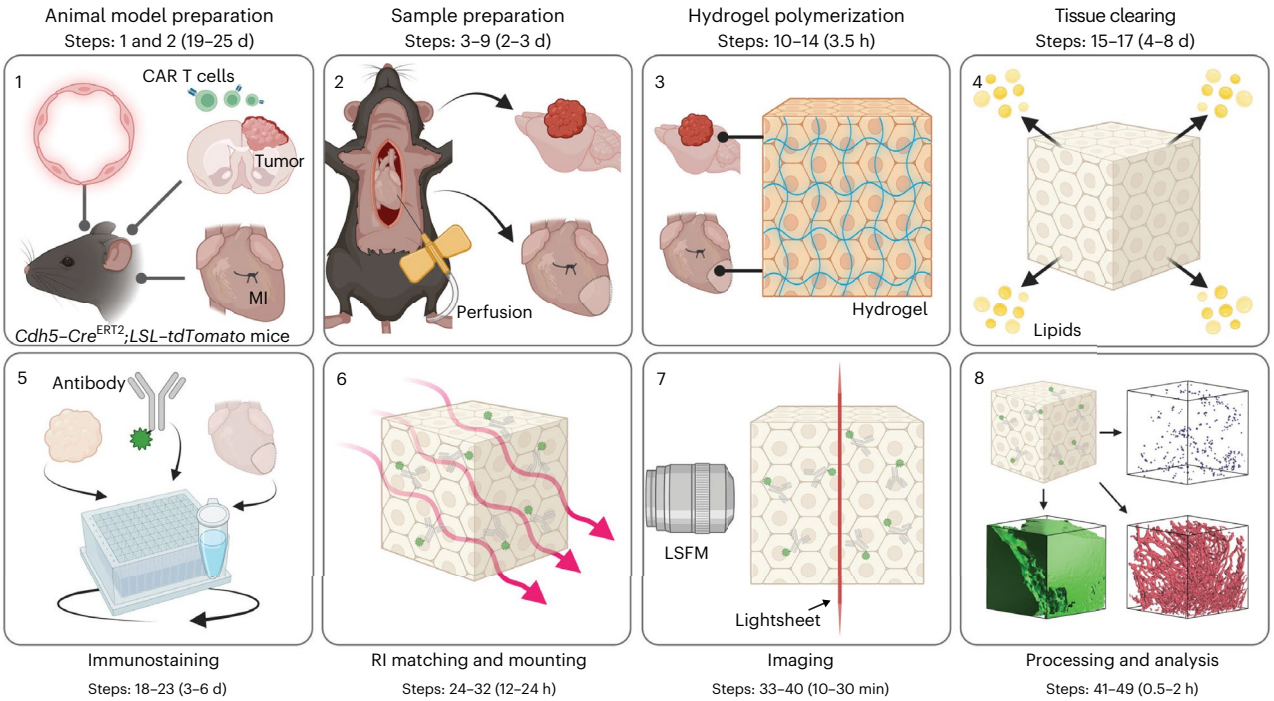

Fig. 1 | Overview of the protocol. Overview of the experimental design involved in this protocol. The procedure is segmented into several essential steps, including animal model preparation for tumor and MI induction, sample preparation, hydrogel polymerization for the preservation of biomolecular structures and functionalities, tissue semi-clearing for removing lipids and making the tissue transparent, sample immunostaining, RI matching and mounting for reducing light scattering and improving image clarity, tissue imaging using LSFM, and data processing and analysis. Figure created with BioRender.com.

Animal model and sample preparation

To rigorously visualize vasculature, we used an EC-specific tamoxifen-inducible tdTomato expression system, namely, *Cdh5–Cre*^{ERT2}*;Rosa–LSL–tdTomato* mice on C57BL6 background as tissue sample donors. We tracked vascularization in physiological conditions, such as in normal brain and heart tissues, and in pathological settings including cancer and CVD. As we recently published, for the cancer model, glioblastoma (GBM), the most common type of malignant primary brain tumor, was induced in *Cdh5–Cre*^{ERT2}*;Rosa–LSL–tdTomato* mice by orthotopic transplantation with firefly luciferase (fLuc)-expressing mouse tumor cells[7]. Tumor growth was validated by whole-body bioluminescence imaging. For the CVD model, MI was induced by ligation of left anterior descending coronary artery[11]. Compromised cardiac function was verified by echocardiogram.

To evaluate tissue hypoxia and perfusion, pimonidazole HCl (Hypoxyprobe) and fluorescent dye-conjugated lectin were intravenously injected, respectively, before tissue collection. Considering that plasma half-life of Hypoxyprobe in mice is ~25 min, we kill the animals 30 min after the probe injection. It is worth noting that although the unspecific binding of pimonidazole HCL to tissue postmortem is low, a gap ≥25 min between Hypoxyprobe administration and killing is needed for the unbound Hypoxyprobe to be fully metabolized. For lectin injection, a gap of at least 5 min is needed for a uniform distribution across the circulation system.

To achieve optimal perfusion and fixation of the tissue samples, it is crucial to utilize a compound perfusate that facilitates thorough penetration of the hydrogel solution while preserving tissue architecture. This protocol recommends initiating perfusion with a PBS + ethylenediaminetetraacetic acid (EDTA) perfusate to flush out blood retention, a significant source of autofluorescence in the samples. The subsequent use of an acrylamide–paraformaldehyde (PFA) perfusate (AP) aims to maximize preservation of molecular and cellular structure and shorten the time required for tissue fixation and hydrogel embedding (Fig. 2).

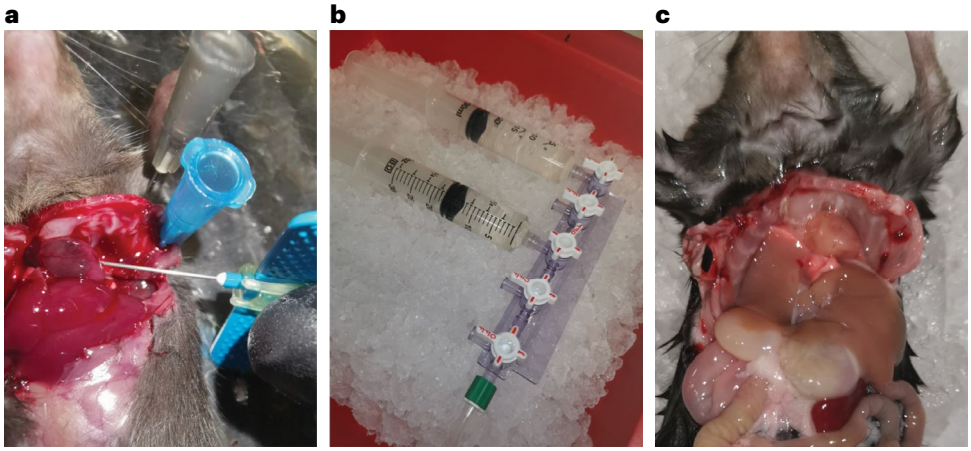

Fig. 2 | Tissue perfusion for sample preparation. A system for transcardial perfusion. **a**, A 25 G BD vacutainer needle was inserted into the left ventricle of the heart (Step 6). Mice were imaged before perfusion. **b**, The perfusion needle was connected to a stopcock manifold with inlets connected to two 30 ml syringes loaded with the respective perfusates (anticoagulant perfusate and AP solution). Perfusates were placed on ice and injected manually by pushing the syringes (Steps 6–7). **c**, Mice were imaged after perfusion. Successful perfusion can be verified by change in the color of the heart and liver (from bright or dark red to light salmon or yellow) and stiffening of limbic muscles (Step 7).

The polymerized hydrogel in the vasculature and heart aids in maintaining lumen integrity and prevents the collapse of thick arteries or fragile areas affected by MI during the semi-clearing process. The duration of incubation in the AP solution is critical for achieving proper fixation and stabilization of the tissue samples. The ideal incubation period should be optimized based on the specific experimental requirements and the type of tissue being analyzed. Adjustments to the incubation length may be necessary depending on the sample size to ensure adequate infusion. In the case of tumor tissue perfused with the AP solution, this protocol recommends a 2–3 d incubation for the adopted general sample dimensions. However, larger or denser samples may require an extended incubation period. It is important to avoid over-infusion of the AP solution over an extended period, as excessive cross-linking can make the samples more difficult to clear in the subsequent steps.

Hydrogel polymerization

In this step, we perform the heat initiation of hydrogel monomer solution infused into the tissue. The tissue, along with the monomer solution, is then heated to 37 °C to initiate the polymerization process. This results in a firm, yet transparent, hydrogel–tissue hybrid that retains the original structure of the tissue and is compatible with the subsequent semi-clearing and staining steps of the protocol.

The presence of oxygen is known to inhibit the high-temperature polymerization step in hydrogel-based semi-clearing methods. For this step, we used a hypoxic tissue culture chamber to create this environment for the convenience of controlled oxygen level, humidity and temperature. Alternatively, based on the availability of equipment, the following procedure can be implemented: (1) degas the sample in a hydrogel solution using a vacuum chamber; (2) create a seal to prevent gas exchange by adding a layer of low-density liquid, such as peanut oil; and (3) incubate the layered sample in a 37 °C water bath.

After the high-temperature polymerization step, a layer of acrylamide gel may form around the sample. This layer needs to be carefully removed to ensure proper exposure of the tissue samples for subsequent semi-clearing and staining procedures. To achieve this without risking damage to the sample, a simple technique involves placing the gel-encapsulated samples on top of a piece of lens cleaning paper tissue and gently rolling the samples around the paper tissue. The larger surface area created by the paper fibers causes the acrylamide gel to stick and tear off, leaving only the fixed and gel-embedded tissue (Fig. 3a,b).

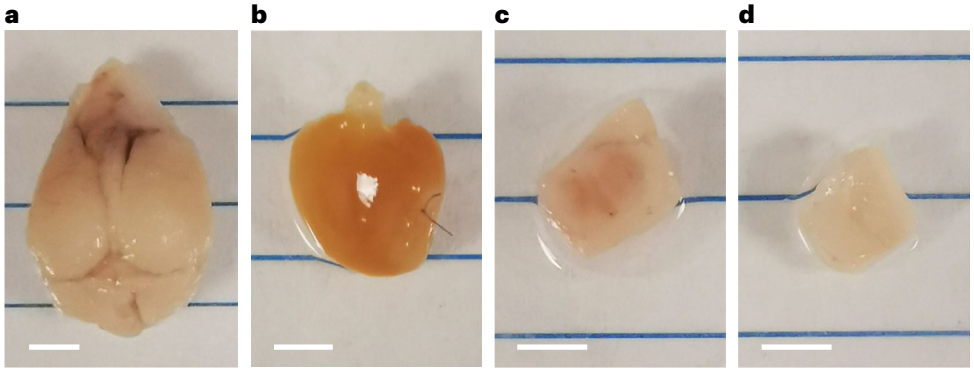

Fig. 3 | Sample processing by hydrogel polymerization. a–d, Samples imaged after hydrogel polymerization (Steps 13–14) for whole-brain tissue with GBM tumor (**a**), whole-heart tissue with MI (**b**), trimmed GBM tumor tissue (**c**) and normal brain tissue (**d**). Scale bars, 3 mm.

To streamline and standardize the processes of semi-clearing and staining as well as getting a better transmittance along the *z* axis for pigmented tissues, it is advisable to cut and trim the tissue samples into small, uniform pieces immediately after gel polymerization (Fig. 3c,d). This approach facilitates efficient penetration of clearing and staining reagents, resulting in faster and more consistent processing for samples of similar volumes. In our protocol, we utilized 96-well plates as staining vessels, and therefore recommend tumor samples with dimensions of ~27 mm^3 (3 × 3 × 3 mm) to accommodate the 7 mm inner diameter of the wells. It should be noted that sample pieces with dimensions less than 3 mm are not recommended as they would not provide at least one unbiased ROI of 1 × 1 × 1 mm. For hearts of 8- to 10-week-old mice, trimming is typically not required as they can fit into the wells of a 96-well plate without modification. However, for larger samples that cannot be trimmed, larger staining vessels and longer clearing/staining times must be employed to accommodate their size.

Tissue semi-clearing

For the tissue semi-clearing step, researchers have the option to choose between electrophoretic tissue clearing (ETC) and passive clearing methods. ETC offers a faster workflow by actively repelling sodium dodecyl sulfate (SDS) micelles out of samples, but for higher-quality images, passive clearing is always preferred.

Passive clearing generally takes a long duration to achieve an ideal clearing outcome but can be accelerated by implementing continuous agitation and maintaining a consistent temperature. A commonly used setup involves placing conical centrifuge tubes with samples and clearing buffers in a heated shaker typically used for bacterial culture. For a compact setup, we inserted five separators made from cut-down sample vials into a 50 ml conical tube, creating six sample compartments that share the 50 ml clearing buffer (Fig. 4a). This configuration allows for parallel heated clearing of 24 samples using a 4 × 50 ml adaptor and a Thermomixer C heated shaker (Fig. 4b). In this setup, 3D-printed sample separators can be utilized, with stereolithography 3D printing preferred over conventional fused deposition modeling (FDM) printing to avoid *Z*-banding that could potentially damage the samples during agitation.

Although passive clearing is preferred due to its simplicity and lower risk of tissue damage, it takes a longer time to achieve satisfactory results compared with ETC. In this protocol, we have expedited the process by reducing the sample size to a relatively small and uniform volume. For trimmed healthy brain or GBM tumor samples with dimensions of ~4 mm on each side, optimal clearing can be achieved within 3–4 d, and ~7 d for a mouse heart (Fig. 4c–e). However, for larger samples such as whole mouse brains or tumor-bearing brains, the process may take up to 3 weeks.

For ETC, tissue samples should remain relatively stationary, with their orientation remaining unchanged throughout the process. Common laboratory supplies such as tissue cassettes or cell strainers can be improvised as ETC sample holders. To accommodate parallel

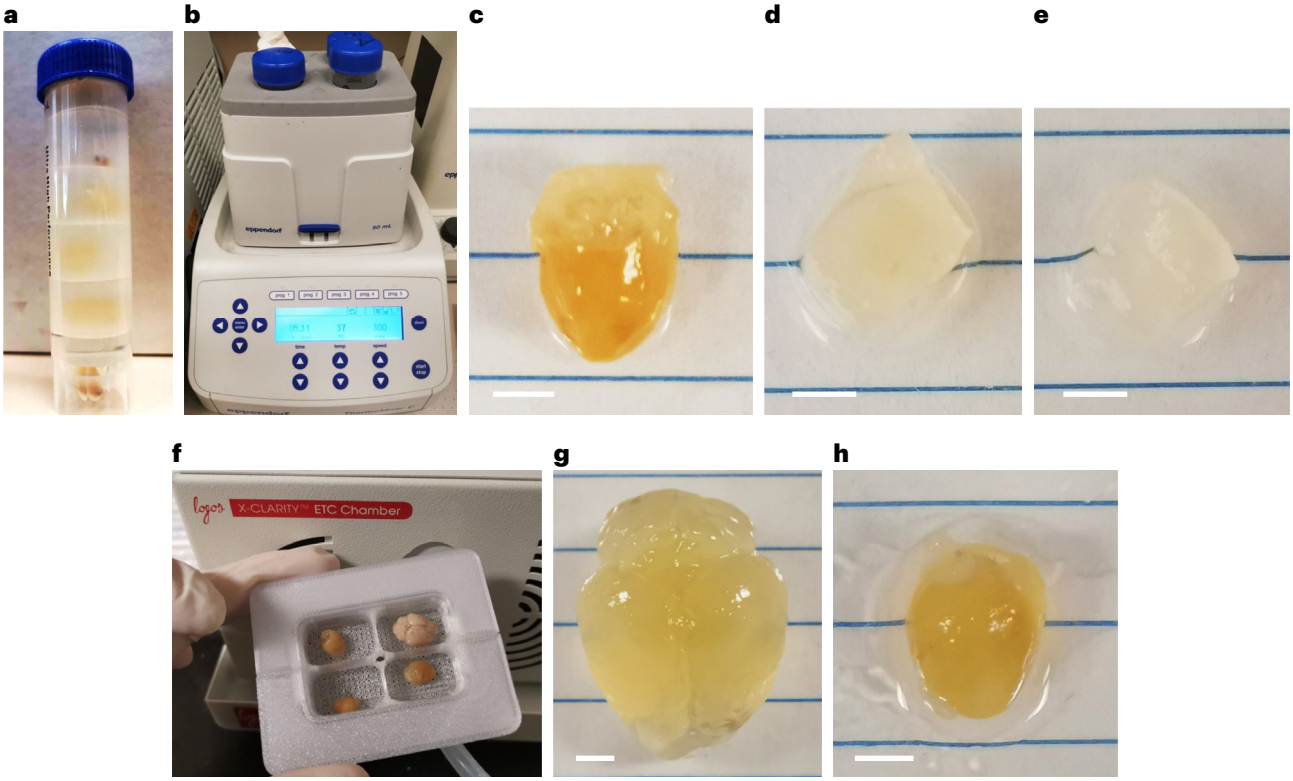

Fig. 4 | Sample processing by tissue semi-clearing. a–**e**, Tissue samples were subjected to passive tissue semi-clearing. Samples were placed in a compartmentalized 50 ml conical tube (**a**) and incubated in a thermomixer (**b**) (Step 16A(i)). Normal heart sample with MI was imaged 7 d after semi-clearing (**c**) (Step 16A(i–iii)). Trimmed GBM tumor (**d**) and normal brain samples (**e**) were imaged 4 d after semi-clearing (Step 16A(iii)). **f**, Tissue samples were subjected to ETC semi-clearing in a polycarbonate 3D-printed ETC tissue holder (Step 16B(i)). **g**, Healthy whole-brain sample after 1 d ETC (Step 16B(iii)). **h**, Healthy whole-heart sample after 2 d ETC (Step 16B(iii)). In **c**–**e**, **g** and **h**, scale bars, 3 mm.

ETC across many smaller samples, sample holders for ETC can be designed and 3D printed to fit specific needs. As an example, we have designed an ETC sample holder for X-CLARITY system that can hold eight tissue pieces for simultaneous semi-clearing of brain and heart tissues (Supplementary Software 1 and Fig. 4f–h). Note that the material for ETC sample holder must be nonconductive and temperature- and chemical-resistant. For FDM 3D printing, polycarbonate is an ideal option. For stereolithography 3D printing, temperature- and chemical-resistant resin can be used. Sufficient tolerance should be reserved when designing such sample holders to avoid compression of tissue when samples start to expand in all directions.

ETC typically requires specialized equipment to control the electric field and regulate buffer circulation temperature. However, ETC can cause tissue yellowing and expansion when samples are exposed to excessive temperature or electrical current. This poses a significant risk, particularly for pathological samples such as tumors or hearts with MI, as the density and rigidity variations in the tissue can result in nonuniform expansion, leading to inaccurate tumor boundary images. As a result, images of tumor boundary may lose accuracy. Mouse heart post-MI may also rupture along the thin and fragile MI area, or turning the affected ventricle chamber inside out. It is crucial to empirically determine the optimal ETC settings for different tissue types, always starting with a safer setting of higher flow rate and lower temperature and voltage.

Immunostaining

The effective and specific labeling of target molecules or cells relies on critical factors such as the choice of antigen, antibody concentration, staining time and staining temperature.

Optimization of these parameters is essential to obtain high-quality imaging results and ensure reliable data analysis. To enhance penetration depth into the sample, staining agents with smaller sizes are preferred. Whenever possible, VHH fragments (nanobodies) or F(ab')2 fragments should be chosen over whole IgG antibodies. Additionally, when staining samples with a high abundance of Fc receptors, such as spleen or GBM tumors containing numerous monocytes or macrophages, the use of an Fc receptor blocker alongside the staining antibody is recommended to prevent nonspecific binding.

To establish a low-profile staining setup, we regulated the volume of samples by utilizing a 96-well plate sealed with a qPCR plate sealing sticker. This setup facilitates the easy transfer of samples across different temperature stages and allows for smaller volumes of staining reagents (~200 µl/well). Consequently, it reduces costs and minimizes waste, which is particularly advantageous when working with multiple samples or limited/expensive reagents. In this protocol, we adopted a multistage staining approach to enhance antibody penetrance and binding. The samples were continuously agitated on an orbital shaker and subjected to temperature shifts between 37 °C, 4 °C and 25 °C (room temperature). This temperature variation facilitates changes diffusion rate and sample volume, allowing for better absorption of staining agents and stabilization of specific binding. It is important to adapt this step to accommodate samples with different sizes, densities and target abundances.

RI matching and sample mounting

The choice of RI-matching media plays a crucial role in achieving optimal imaging quality. By matching the RI of the sample to that of the immersion medium, light scattering can be substantially reduced. It helps in creating a more uniform medium for the light to pass through, enabling the excitation light sheet to penetrate deeper into the tissue while maintaining the sharpness of the image. Without RI matching, there can be considerable distortion and reduction of the signal due to light scattering in the tissue, leading to an inaccurate representation of the sample. In this protocol, we utilized 88% histodenz[27] as the RI-matching solution (RIMS) to ensure high-clarity samples and spatially accurate feature analysis (Fig. 5a–c). Maintaining the appropriate RI of the mounted sample is essential for obtaining high-quality images as RI across the tissue sample and the light path must be matched, to prevent photons from scattering. Therefore, it is important to homogenize the histodenz solution stock and inspect its RI with a refractometer before use, as evaporation and precipitation can lead to inconsistencies in the solution and affect the desired RI of 1.46. Histodenz has radiopaque properties that enable clear visualization of blood vessels, organs and tissues. Additionally, the fluidity of the 88% histodenz RIMS we use improves the imaging quality. More viscous solutions decrease the transparency, are more prone to capture bubbles or dirt and impede the sample handling in the chamber. To address the high cost of histodenz solution, recycling can be achieved through 0.45 µm filtration. Adjusting the RI deviation may be needed for recycled solution as its RI may increase (by evaporation when stored in a big vessel) or decrease (diluted by PBS in the hydrogel-embedded tissue samples). This can be accomplished by adding water, reducing the solution through evaporation or spiking in additional histodenz.

To ensure stable mounting and precise positioning of samples during imaging, we designed sample holders compatible with the Zeiss Z.1 light sheet microscope and our sample shape holder (Supplementary Software 2). This strategy can be adapted to accommodate different microscope models and various types of tissues. Transparent polylactic acid (PLA) was chosen as the material for producing these sample holders using FDM 3D printing. PLA exhibits a RI that closely matches that of RIMS and RI-matched samples[39]. This characteristic helps to minimize internal reflection and refraction within the imaging chamber, making it a preferable choice over other FDM printing materials, as well as metal or glass sample holders.

For mounting irregularly shaped or fragile samples, we developed a method that utilizes a 2% agar in RIMS gel to encapsulate RI-matched samples. This approach enables us to preserve the original shape and orientation of the samples, while providing an environment conducive to RI-matched imaging (Fig. 5d–g). The mechanical properties of agar in RIMS gel are more durable compared with agar in water gel or low-melting point agar gel. Consequently, this gel

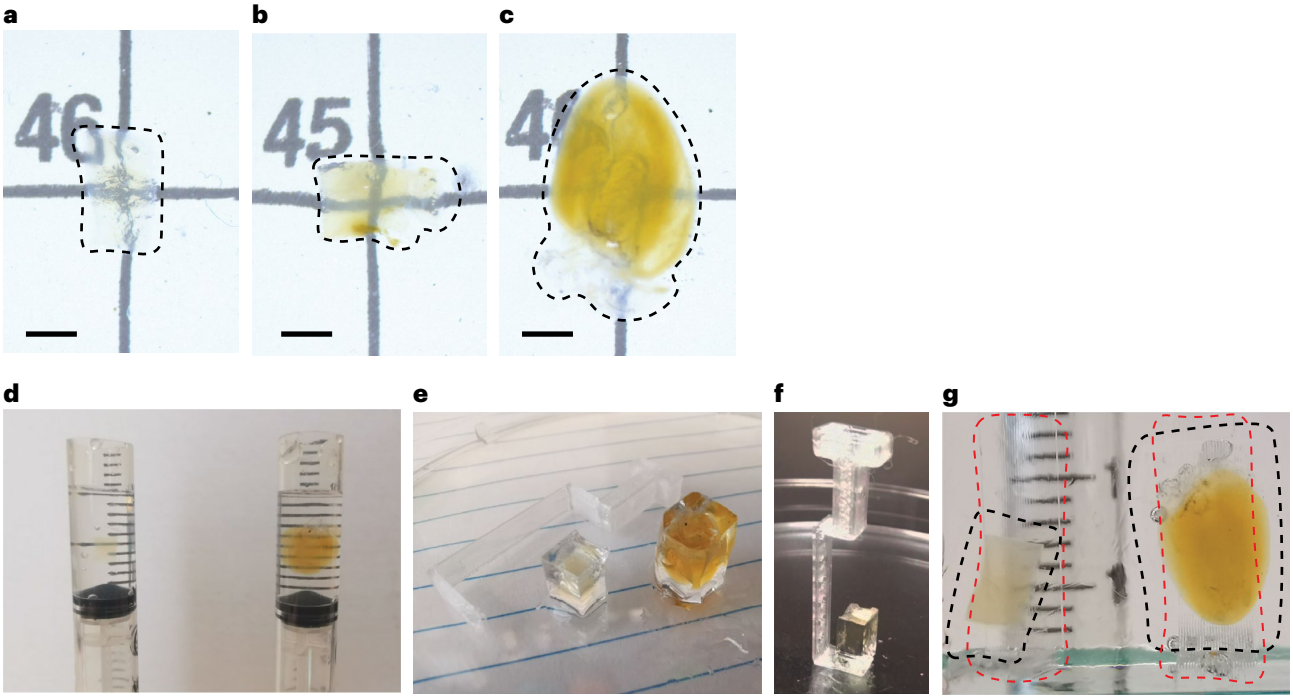

Fig. 5 | RI matching and sample mounting. a–**c**, Tissue samples were processed by RI matching (Step 24). Trimmed healthy brain tissue (**a**), trimmed GBM tumor tissue (**b**) and whole-heart tissue (**c**) were imaged. Dashed lines indicate the edges of tissue samples. Scale bars, 3 mm. **d**–**f**, Tissue samples were mounted. Samples were subjected to RIMS–agar encapsulation in trimmed 3 ml syringes (**d**) (Step 25). Sample blocks were encapsulated on a 3D-printed tissue holder (**e**) (Steps 26–30). Sample encapsulated in RIMS–agar is fixed to a 3D-printed sample holder by glue (**f**). **g**, Encapsulated sample blocks were fixed to a 3D-printed tissue holder, immersed in RIMS (Steps 31–32). Black dashed lines outline sample blocks. Red dashed lines outlines tissue holder.

formulation offers excellent protection for fragile samples that cannot be mounted by using glue and reduces sample wobbling during image acquisition.

Imaging

The Zeiss Z.1 lightsheet microscope, although having a smaller imaging volume compared with other commercially available or custom-made lightsheet microscopes, offers the advantage of rapid imaging of sample sizes recommended by this protocol, while producing high-resolution images. However, it is crucial to acknowledge the limitations in sample size to ensure the acquisition of accurate and reliable data. Under tile scan mode, we have managed to acquire whole-hemisphere imaging of a normal mouse brain (Extended Data Fig. 1) processed by the sample preparation and semi-clearing protocol here, where *z*-axis transmittance is not a problem without any optical obstruction, such as the ones that can be commonly found in tumor tissues. As hydrogel-based semi-clearing is moderately expansive in nature, whole-brain imaging is not feasible using this setting as the sample will hit on the wall sample chamber during the scan. For bigger samples, a lightsheet microscope with a bigger imaging volume or a clearing technique that can cause sample shrinking (e.g., organic solvent based) must be adopted. Moreover, careful consideration of the compatibility between laser/filter set combinations and the fluorophore panel is essential for successful image acquisition and to minimize bleedthrough between acquisition channels. This will contribute to the overall quality and reliability of the obtained data. Therefore, optimizing these parameters and understanding their impact is critical for obtaining robust and meaningful results.

Imaging fluorophores with a short excitation wavelength (e.g., 405 nm laser) presents additional difficulties due to the high absorbance of water and various biological molecules in short wavelength visible light[40]. This results in reduced penetrance compared with longer

wavelengths, posing a challenge. In the case of high-content imaging samples requiring multiband excitation, it is advisable to use higher laser intensity and longer exposure time for the short wavelength channels (e.g., blue fluorescent proteins or dyes).

Data processing and analysis

The efficient management and storage of data generated from LSFM is crucial due to the substantial size of the datasets, which can range from hundreds of gigabytes to terabytes depending on sample size, resolution and number of acquired channels. To ensure streamlined data processing and analysis, it is important to employ proper data management and storage strategies. Additionally, investing in appropriate computing resources facilitates efficient data processing, analysis and storage, thereby enabling faster and more reliable research outcomes. In the case of a local workstation setup, employing a storage configuration that prioritizes fast read/write speeds, such as a Redundant Array of Independent Disks system utilizing multiple solid-state drives, effectively reduces the processing time required for handling large batches of high-resolution images.

To execute the methodology outlined in this protocol, we utilized Imaris software to preprocess and analyze the acquired images. Imaris software (v10.0) offers artificial intelligence-assisted feature filtering and tracing capabilities, which greatly enhance the efficiency and accuracy of processing large-scale imaging data. On the basis of Imaris, we performed analysis of vascular structure and perfusion in hearts (Fig. 6); tumor vascularization, perfusion and hypoxia (Fig. 7); T cell infiltration and immune composition in tumors (Fig. 8); and vascularity and immunity analysis (Figs. 9 and 10), with an optimized workflow (Fig. 11 and Extended Data Fig. 3). In addition, it is worth noting that achieving the same goals is possible by utilizing other commercial or open-source tools such as Fiji, Vaa3D or Amira.

Accurately correcting image voxel size is critical to account for potential sample shrinking or expansion that may occur during the tissue semi-clearing and staining processes.

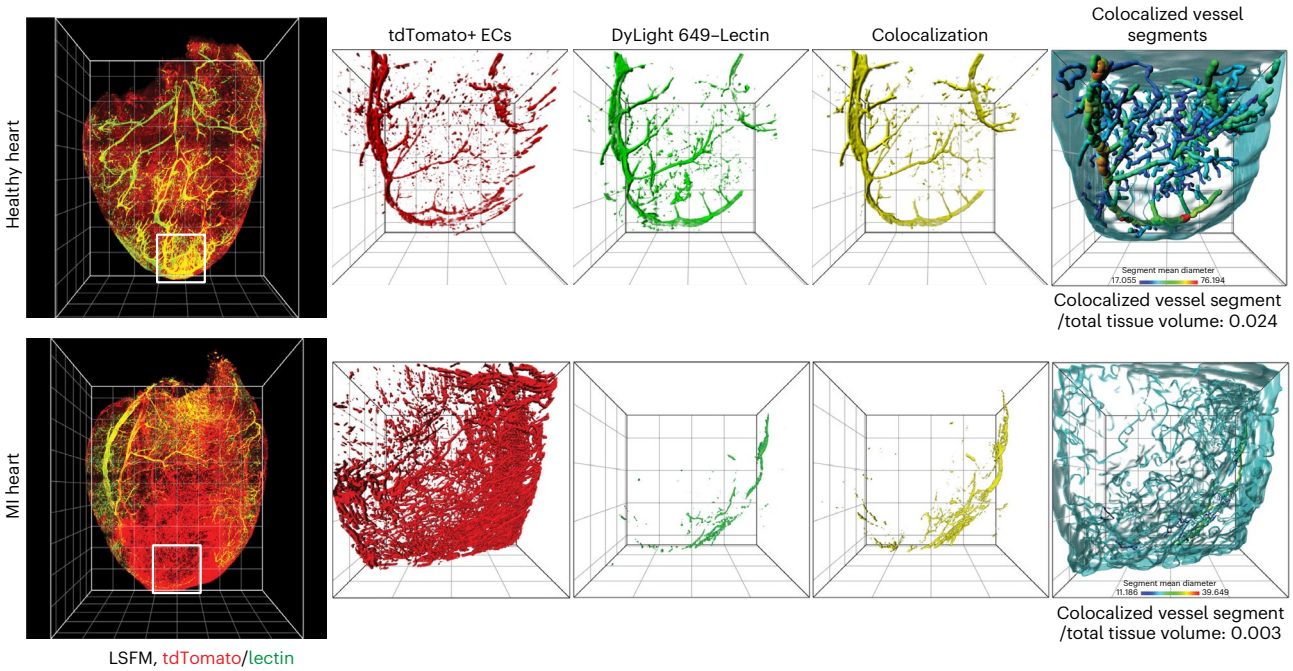

Fig. 6 | LSFM analysis for vascular structure and perfusion in hearts. Heart samples were collected from lectin-perfused healthy or diseased *Cdh5–Cre*^{ERT2}; *LSL–tdTomato* mice 3 weeks post-MI, followed by tissue semi-clearing and LSFM imaging. Left, whole-heart images. Each minor tick on the grid represents 1 mm. White boxes represent the ROI selected for zoomed-in views. Right, zoomed-in view of healthy left ventricle and MI areas. Each minor tick on the grid represents 500 µm. For colocalized vessel segment panels, cyan surface represents actual tissue volume. Registered vessel segments are color coded by mean diameter of the segments.

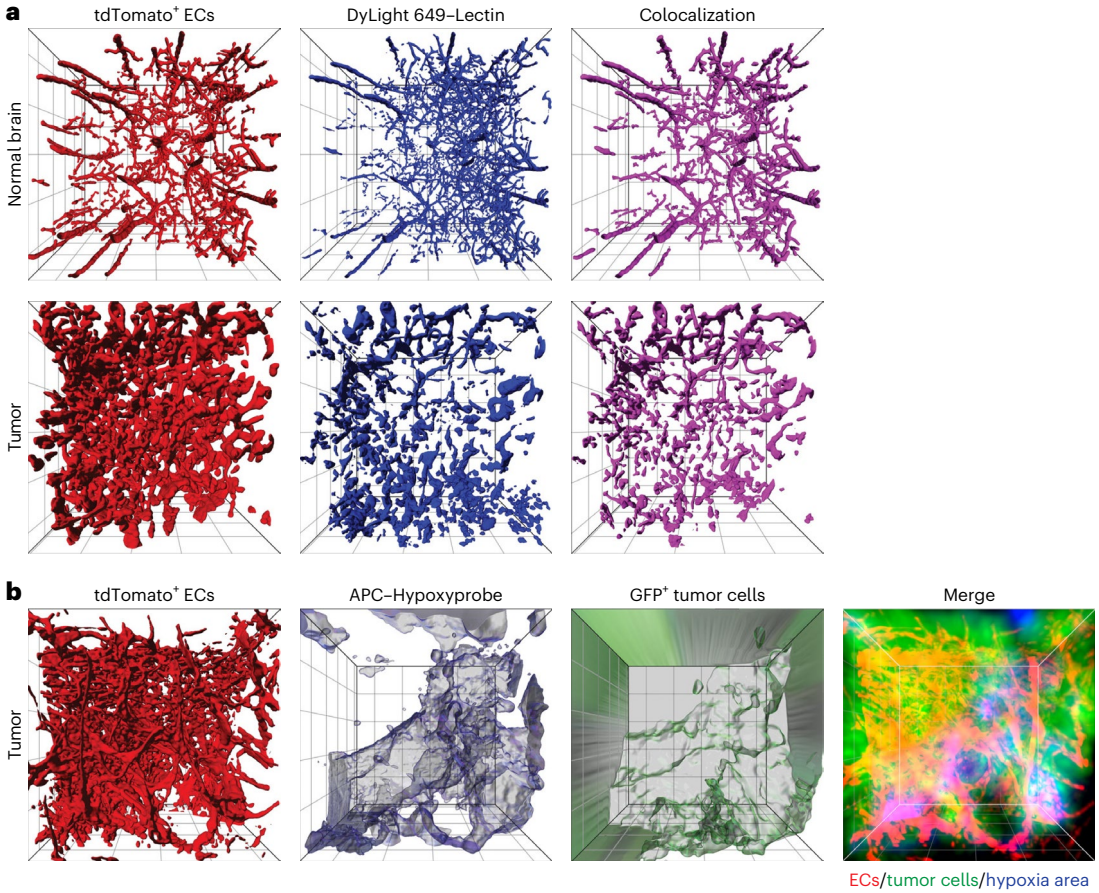

Fig. 7 | LSFM analysis for tumor vascularization, perfusion and hypoxia. GBM was induced in *Cdh5–Cre*^{ERT2};*LSL–tdTomato* mice, followed by perfusion with lectin and hypoxyprobe. Normal brain and tumor samples were subjected to tissue semi-clearing and imaged by LSFM. GFP$^+$ tumor cells and hypoxia region signal are visualized as transparent surface volume objects; other features are visualized under the normal shading mode. Each minor tick on the grid represents 200 µm. **a**, Analysis for vascular perfusion. **b**, Analysis for vascularization and hypoxia.

The semi-clearing process often leads to an isotropic expansion of the sample. While the RI-matching step in RIMS may shrink the samples, the overall change in dimensions is usually expansive. These alterations, if not accounted for, could introduce inaccuracies in the subsequent imaging and interpretation stages. By meticulously tracking these size changes, appropriate adjustments can be integrated into the image processing stages, ensuring that the imaging outcomes accurately reflect the original histology samples. As a recommended practice, we propose measuring the dimensions of samples both before hydrogel embedding and after RI matching. By calculating the difference between these measurements, an expansion/shrinkage factor can be obtained. Applying this factor to the acquired image allows for volume adjustment, ensuring that the image accurately represents histological dimensions. This approach enhances the reliability and accuracy of the histological analysis, ensuring consistency between the observed and actual state of the tissue samples.

The choice of ROI is a critical factor in tissue imaging, particularly when studying specific pathologies such as mouse GBM or MI. In the examples provided in this protocol, our objective is to exclude nontumor areas in GBM samples or focus on the infarction region in heart samples. Standardizing image dimensions for statistical purposes is also crucial, and our protocol suggests typical measurements of 1 × 1 × 1 mm for GBM or brain tissue samples and 2 × 2 × 2 mm for left ventricle or MI regions in heart samples. This volume of ROI was decided upon to

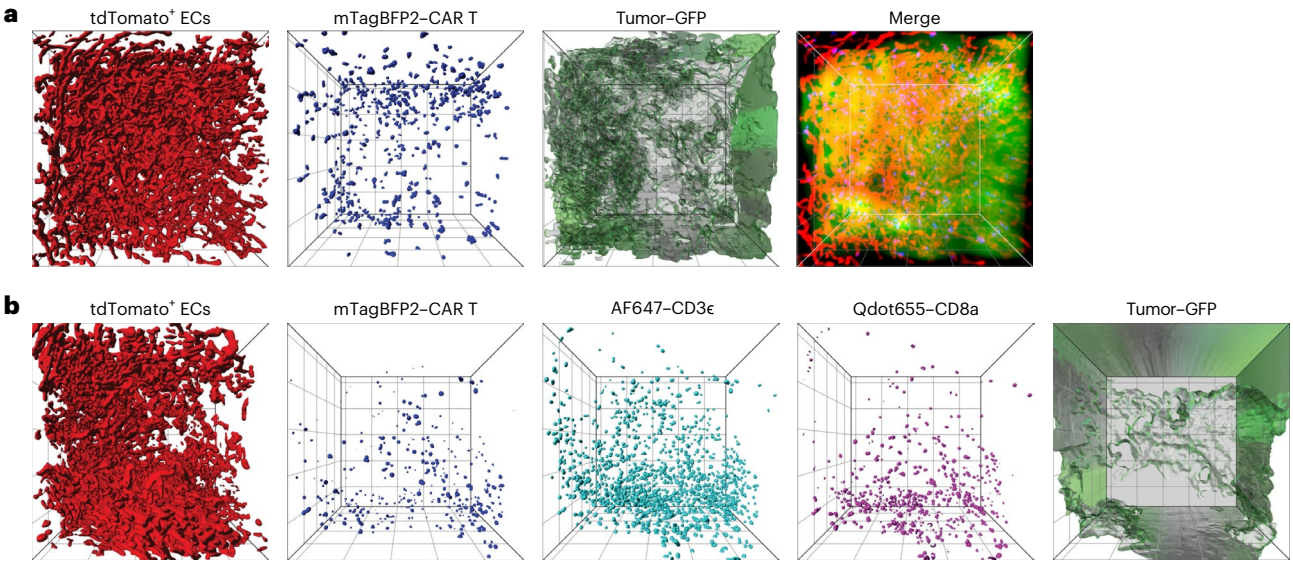

Fig. 8 | LSFM analysis for CAR T cell infiltration and immune composition in tumors. GBM was induced in *Cdh5–Cre*^{ERT2}*;LSL–tdTomato* mice, followed by intravenous injection with mTagBFP2$^+$ CAR T cells. Tumor samples were subjected to tissue semi-clearing, immunostaining and imaged by LSFM. GFP$^+$ tumor cells are visualized as transparent surface volume objects; other features are visualized under the normal shading mode. Each minor tick on the grid represents 200 µm. **a**, Analysis for vascularization and CAR T cell infiltration. **b**, Analysis for vascularization and infiltration of CAR T cells, and CD3ε$^+$ and CD8a$^+$ T cells.

achieve a better balance between content coverage and computational complexity, and it should be adjusted based on the actual sample volume and the specific features of interest to be observed.

The 'Image Processing' module in Imaris is then utilized to deconvolute each channel based on the correct objective lens numerical aperture, medium and specimen RI, and emission wavelength. Deconvolution helps to correct optical aberrations, improving the visibility of details and structures in 3D images, and is always recommended for this protocol. Any nonuniformity in average intensity along the *z* axis due to factors such as tissue coloring or inconsistent laser illumination can be rectified using the 'Normalize Layers' function. Additionally, a significant amount of background or autofluorescence can be reduced by employing the 'Background Subtraction' function, further improving the clarity and quality of the resulting image.

Specific features are then highlighted and analyzed. For example, samples with conjugated lectin injected can be analyzed by the 'Coloc' module to calculate and visualize the colocalization of tdTomato$^+$ vasculature and lectin-labeled perfused vasculature (Figs. 6 and 7a). Objects are created for feature registration and statistical computation, using object creation functions such as 'Surfaces', 'Filaments' and 'Spots' to analyze global, vascular and spot features respectively. Specific criteria for thresholding, smoothing and filtering are defined, and the resulting statistical values are exported for further analysis. Specifically, Imaris offers machine learning methods for more efficient and accurate blood vessel segment recognition in the filament construction module. Once seed points have been generated using the 'Multiscale Points' function, the 'Segment Classification' step is employed. Some generated segments are then categorized into 'Keep' and 'Discard' training sets. Machine learning algorithms will then predict which segments should be kept and which should be discarded, based on the models generated from the training set. This feature dramatically enhances the accuracy and efficiency of vessel segmentation, enabling researchers to obtain more reliable results from their imaging data.

Finally, sample or object-specific criteria are calculated based on the exported statistics. Throughout the protocol, maintaining consistent image processing settings is crucial to ensure data integrity and comparability across all samples within a single experiment. Regular quality

checks and troubleshooting are necessary to address potential issues with noise, uneven lighting or inaccurate measurements. This rigor in the image processing pipeline ensures that the generated results are reliable, accurate and scientifically robust.

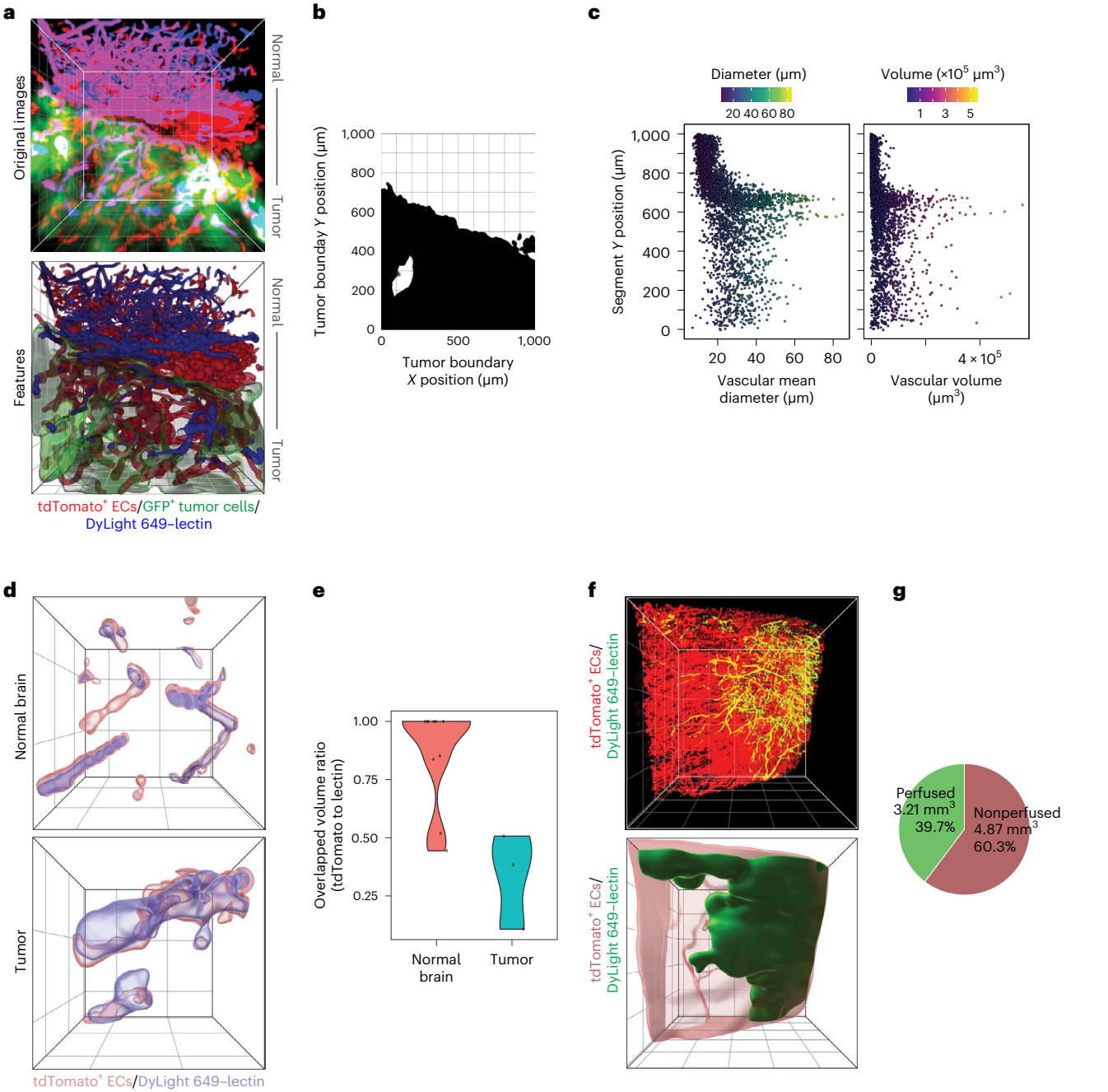

Fig. 9 | Imaging analysis for vascularity. a–**e**, GBM was induced in *Cdh5–Cre*^{ERT2};*LSL–tdTomato* mice, followed by perfusion with lectin. Tissue samples were subjected to tissue semi-clearing and imaged by LSFM. Vascular perfusion in tumor and adjacent normal tissue was analyzed (**a**–**c**). Representative images (**a**). Each minor tick represents 100 μm. Boundary of the tumor object projected on the *XY* plane (**b**). Mean diameter and volume of tdTomato$^+$ segment are plotted against Y position (**c**). Vessel leakage in normal brain and tumor was analyzed (**d**,**e**). Representative images (**d**). Each minor tick represents 100 μm. Overlapped volume ratio of tdTomato vessel to lectin is plotted (**e**). Lower means more volume of lectin signal exposed without tdTomato coverage. **f**,**g**, MI was induced in *Cdh5–Cre*^{ERT2};*LSL–tdTomato* mice. Three weeks after MI induction, heart tissues were subjected to tissue semi-clearing and imaged by LSFM. Vascular perfusion in the border zone was analyzed. Top, LSFM images. Bottom, surface object was generated for each channel by a smoothing factor of 20 μm with low threshold to detect boundary of each feature (**f**). Total tissue volume and perfused volume were calculated (**g**).

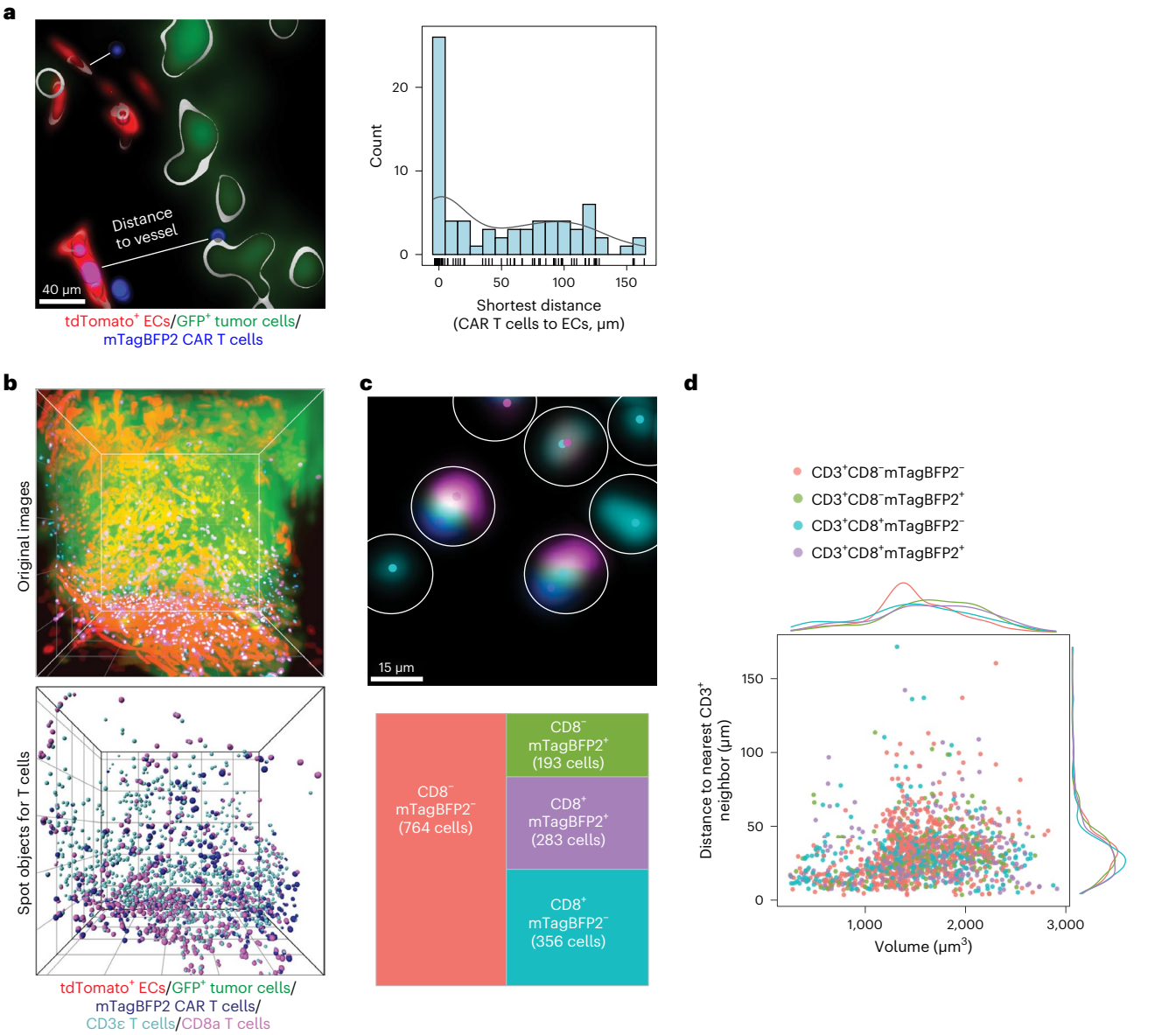

Fig. 10 | Imaging analysis for tumor T cell immunity. GBM was induced in *Cdh5–Cre*^{ERT2};*LSL–tdTomato* mice, followed by intravenous injection with mTagBFP2$^+$ CAR T cells. Tumor samples were subjected to tissue semi-clearing and imaged by LSFM. **a**, Distance of mTagBFP2$^+$ CAR T cells to tdTomato$^+$ vessels. Left, representative image. Right, distance of all mTagBFP2$^+$ CAR T cells to their closest tdTomato$^+$ vessels was collected over a volume of 500 × 500 × 500 μm tumor tissue. **b**–**d**, Composition and distribution analysis of T cells. Representative LSFM images (**b**). Each minor tick represents 200 μm. Single T cells with multiple signals were parsed based on distance between spot objects (**c**). Top, representative image. Each white circle represents one cell. Bottom, subtype composition of CD3$^+$ T cells. A plot of cell volume versus distance to nearest neighbor cells in CD3$^+$ T cells (**d**).

Materials

Reagents

Samples

- We utilized animals expressing fluorescent proteins in endothelial lineage cells for this protocol. The objective was to visualize endogenous vascular ECs in healthy or pathological settings. *Cdh5–Cre*^{ERT2};*Rosa–LSL–tdTomato* mice were generated by crossing *Rosa–LSL–tdTomato* mice (Jackson Laboratory, strain no. 007914) with *Cdh5–Cre*^{ERT2}

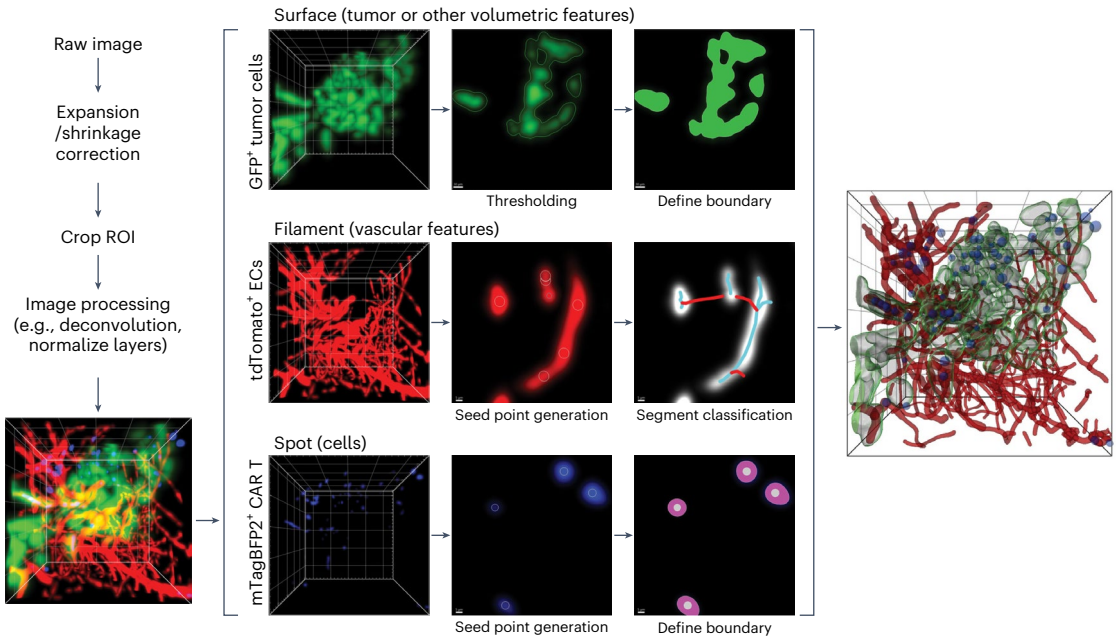

Fig. 11 | Workflow for image processing and feature registration. Voxel sizes of raw images are first corrected for the potential expansion of samples. Images are then cropped and processed to increase the signal-to-noise ratio of the ROI. Surface objects are used to register volumetric features, such as tumor and hypoxic area. The correct threshold must be set to recognize object boundary accurately. Filament objects are used to register vascular features, such as tdTomato$^+$ ECs and lectin-perfused vessels. After seed point generation, machine-learning-based segment classification is used to determine whether a segment generated between seed points is valid (red segments are in the 'Discard' set, cyan segments are in the 'Keep' set). Spot objects are used to register cellular features, such as labeled CAR T cells or stained immune cells. After seed point generation, correct boundary setting by thresholding is necessary for correct spot diameter measurement. Each minor tick represents 100 µm. Middle and right images show local 2D slicer views of each channel. The bottom scale bars for surface generation represent 30 µm and for filament and spot generation 5 µm.

mice (provided by Ralf Adams at the Max Planck Institute). Different endothelial-labeling transgenic mouse strains could be used based on the aim of the study or animal availability

▲ **CRITICAL** The experiments involving animals must be conducted in accordance with the institutional guidelines and applicable governmental and institutional regulations for animal experimentation.

Reagents for animal model preparation

- Tamoxifen (Sigma, cat. no. T5648)
  ▲ **CAUTION** Tamoxifen has potential reproductive toxicity and is toxic if swallowed or inhaled. It should be handled with gloves and protective clothing. Dispose of it as hazardous waste according to local regulations.
- Isoflurane (Akorn Animal Health, NDC no. 59399-106-01)
  ▲ **CAUTION** Isoflurane is dangerous if inhaled and may cause drowsiness, dizziness and respiratory depression. It should be used in a well-ventilated area and stored in a cool, dry place away from heat sources. Any leftover isoflurane or contaminated material should be disposed of in accordance with local regulations.

Reagents for T cell preparation

- mTagBFP2–nLuc$^+$ mouse CAR T cells

Reagents for sample preparation and hydrogel polymerization

- ddH_2O
- Saline (Growcells, Cat. no. MSDW-1000)
- Pimonidazole HCl (Hypoxyprobe, cat. no. HP-200mg)

- Peanut oil (Sigma, cat. no. P2144)
- *Lycopersicon esculentum* (Tomato) Lectin (LEL, TL), DyLight 649 (Vector Laboratories, cat. no. DL-1178)
- 1× PBS (Corning, cat. no. 21-040-CM)
- PFA solution, 4% in PBS (Thermo Scientific, cat. no. J19943.K2)
  ▲ **CAUTION** PFA is toxic and may cause irritation to the respiratory system, skin and eyes. It should be handled in a well-ventilated area, and gloves and eye protection should be worn. It must be disposed of as hazardous waste following local regulations.
- Acrylamide (Sigma, cat. no. A8887)
  ▲ **CAUTION** Acrylamide is a neurotoxin and a potential carcinogen. It can be harmful if inhaled, ingested or absorbed through the skin. Use this chemical in a well-ventilated area, wearing gloves and eye protection. Dispose of acrylamide and acrylamide-containing solutions as hazardous waste in accordance with local regulations.
- VA-044 (Wako Chemicals, cat. no. LB-VA044-50GS)
- UltraPure 0.5 M EDTA, pH 8.0 (Invitrogen, cat. no. 15575020)

Reagents for tissue semi-clearing

- Triton X-100 (Sigma, cat. no. X100-100ML)
  ▲ **CAUTION** Triton X-100 can be harmful if swallowed and may cause skin and eye irritation. Handle it with gloves and eye protection and avoid creating aerosols. Dispose of it according to local regulations.
- SDS (Sigma, cat. no. L4509)
  ▲ **CAUTION** SDS can cause skin and eye irritation and may be harmful if swallowed or inhaled. Use gloves and eye protection, and wash hands thoroughly after handling. Dispose of it according to local regulations.
- Boric acid (Sigma, cat. no. B0394)
- Sodium hydroxide (Sigma, cat. no. S5881)
  ▲ **CAUTION** Sodium hydroxide is corrosive and can cause severe skin burns and eye damage. Handle with care, wearing gloves, eye protection and protective clothing. Neutralize the waste before disposal and dispose of it according to local regulations.
- Polycarbonate 3D printing filament (any; we used 1.75 mm PolyLite by Polymaker)

Reagents for immunostaining

- TruStain FcX (anti-mouse CD16/32) antibody (Biolegend, cat. no. 101320)
- Primary and secondary antibodies (for antibodies we have used, see Table 1)

Table 1 | Antibodies for staining mouse tumor and brain tissue blocks

	Concentration used for staining (μg/ml)	Supplier
Unconjugated primary antibodies		
CD3ε (E4T1B) XP Rabbit mAb	20	Cell Signaling Technology, cat. no. 78588, RRID: AB_2889902
Purified Rat anti-mouse CD8a Antibody	20	Biolegend, cat. no. 100702, RRID: AB_312741
Conjugated primary/secondary antibodies		
F(ab')2-Goat anti-Rabbit IgG (H+L) Cross-Adsorbed Secondary Antibody, Alexa Fluor Plus 647	10	Thermo Fisher Scientific, cat. no. A48285TR, RRID: AB_2896350
Alexa Fluor 647 AffiniPure F(ab')$_2$ Fragment Donkey Anti-Rat IgG (H+L)	10	Jackson ImmunoResearch Labs, cat. no. 712-606-153, RRID: AB_2340696
F(ab')2-Goat anti-Rat IgG (H+L) Secondary Antibody, Qdot 655	10	Thermo Fisher Scientific, cat. no. Q-11621MP, RRID: AB_2556477
Hypoxyprobe Red APC MAb	20	Hypoxyprobe, cat. no. Rat-APC-Mab, RRID: AB_3064885

Reagents for RI matching and sample mounting

- Histodenz (Sigma, cat. no. D2158)
- Sodium azide (Sigma, cat. no. S2002)
  ▲ **CAUTION** Sodium azide is toxic if inhaled, swallowed or in contact with skin. Sodium azide solution can form explosive metal azide in contact with heavy metals. Handle it with gloves and protective clothing. Dispose of sodium azide as hazardous waste according to local regulations.
- Loctite 4851 cyanoacrylate glue (Henkel, cat. no. 37732)
- Agar (Fisher, cat. no. BP160)
- Clear/transparent PLA 3D printing filament (Fillamentum, 1.75mm Crystal Clear PLA)

Equipment

- Orbital shaker or vortex mixer (Thermo Scientific, cat. no. 88882009)
- 37 °C incubator (Panasonic Healthcare, cat. no. MCO-170AICUVL-PA)
- 4 °C fridge (True Refrigeration, cat. no. T-49-HC) or cold room
- pH meter (Thermo Scientific, cat. no. STARA2119)
- Refractometer (Atago, cat. no. PAL-RI)
- 96-well plate (Corning, cat. no. 3603)
- Deep 96-well plate (Sigma, cat. no. BR701340)
- Adhesive PCR plate seals (Thermo Scientific, cat. no. AB0558)
- 1.5 ml microcentrifuge tube (PR1MA, cat. no. PR-MCT15-S)
- 5 ml conical tube (Eppendorf, cat. no. 0030119401)
- 50 ml conical tube (Thermo Scientific, cat. no. 339652)
- Disposable 3 ml syringe (BD, cat. no. 309585)
- Warm water bath (FisherBrand, cat. no. 15-462-2Q)
- Lens cleaning tissue (any)
- FDM 3D printer (Prusa, Prusa i3 Mk3s)

Equipment for syngeneic mEgfrvIII^{+} GBM model

- Stereotaxic injection platform (Braintree Scientific, cat. no. 51730)

Equipment for myocardial infraction model

- Rodent ventilator (Kent Scientific, TOPO Dual Mode Small Animal Ventilator)
- 8-0 Prolene suture (Ethicon, cat. no. 2775G)

Equipment for transcardial perfusion

- 25 G BD Vacutainer blood collection needle (BD, cat. no. 367294)
- Manifold with Luer lock (Avantor, cat. no. MFLX3060043)
- Rotating Luer lock and nut assembly (Fisherbrand, cat. no. 01-000-241)
- Tygon PVC tubing, 1/16" ID (McMaster-Carr, cat. no. 6516T62)
- Disposable 30 ml syringe (BD, cat. no. 302832)
- Surgical scissors (FST, cat. no. 14058-09)

Equipment for hydrogel polymerization

- Hypoxic workstation (Don Whitley Scientific, H35 Hypoxystation)
- Vacuum chamber (Thermo Scientific, cat. no. 5311-0250)

Equipment for ETC

- X-CLARITY ETC Tissue Clearing System (Logos Biosystems, cat. no. C30001)

Equipment for passive tissue clearing

- Thermomixer C (Eppendorf, cat. no. 5382000023) with a 50 ml tube adaptor (Eppendorf, cat. no. 5365000028)
- Sample vials (any of similar size; we used Nalgene cat. no. 6250-0012)

Zeiss Lightsheet Z.1 light-sheet microscope configuration
All samples shown here were imaged using a Z.1 LSFM system (Zeiss) at the University of Pennsylvania Cell & Developmental Biology Microscopy Core (RRID: SCR_022373) with the following configuration:

- Objective: Zeiss 5× EC Plan-Neofluar ×5/0, 16 numerical aperture (NA), working distance (WD) of 10.5 mm for immersion buffer of $n = 1.45$
- Excitation lasers: 405 nm, 488 nm, 561 nm, 638 nm
- Illumination: Zeiss LSFM ×5/0.1 NA objectives; dual side illumination in Pivot mode
- Filter sets: 1. SBS LP 490, EF BP 420-470, EF BP 505-545; 2. SBS LP 510, EF BP 420-470, EF BP 525-545; 3. SBS LP 560, EF BP 505-545, EF LP 585; 4. SBS LP 560, EF SP 550, EF LP 585; 5. SBS LP 640, EF BP 575-615, EF LP 660

Data processing and analysis software

- ZEN (Zeiss)
- Imaris (v.10.0.0, Oxford Instruments)
- Imaris Converter (Oxford Instruments)
- Imaris Stitcher (v.10.0.0, Oxford Instruments)

Reagent setup

Anticoagulant perfusate
Dilute 0.5 M EDTA in 1× PBS to obtain 5 mM EDTA in PBS. This solution works as a perfusate to remove blood from the circulation system. EDTA works as an anticoagulant that prevents blood from clotting by binding calcium ions in the blood. Store and use this solution at room temperature. Prepare at least 20 ml for each mouse.

AP solution
Prepare 8% (wt/vol) acrylamide solution in ice-cold 4% PFA in PBS, then prepare 0.5% (wt/vol) VA-044 solution in ice-cold 4% PFA in PBS. Keep the two solutions on ice. Make 1× AP solution by mixing the two solutions in a 1:1 ratio to make 4% (wt/vol) acrylamide and 0.25% (wt/vol) VA-044 in 4% PFA in PBS. We recommend making fresh AP solutions for each use. Keep the 1× AP solution on ice. Prepare at least 35 ml for each mouse.
▲ **CAUTION** PFA and acrylamide monomer in the solution are toxic. Wear proper protection when preparing the solution. Proper processing of tubes and perfused mouse bodies in contact with AP solution is necessary.

Passive clearing solution
Prepare 4% (wt/vol) SDS and 200 mM boric acid solution in ddH_2O. Adjust the pH to 8.5 with sodium hydroxide. Passive clearing solution can be stored at room temperature for months.

Staining buffer
Prepare 0.1% Triton X-100 solution in 1× PBS. The staining buffer can be stored at room temperature for months.

RIMS
Dilute 88% (wt/vol) histodenz and 0.01% (wt/vol) sodium azide in 1× PBS. Use a refractometer to measure and confirm the RI of the prepared RIMS to be 1.46. RIMS can be stored at room temperature for months.
▲ **CRITICAL** The RI of RIMS is critical to the quality of images. Before each use, homogenize the RIMS stock by shaking it and then check the RI of RIMS with a refractometer. If the RI deviates from 1.46, RIMS can be readjusted by spiking in more histodenz or by dilution with 1× PBS.

RIMS–agar solution
Prepare 2% (wt/vol) agar solution in RIMS in a 50 ml conical tube. Leave the tube uncapped and heat up the solution in the microwave. Observe the heating process, stop the microwave

immediately upon boiling and cap the tube to avoid change in RI by excessive evaporation. Keep the hot solution liquid in a water bath set to 50 °C before mounting the sample. Excessive RIMS–agar solution can be kept at room temperature for at least a month. The solidified solution can be re-liquified by heating before the next use.

Equipment setup

Transcardial perfusion setup

To introduce the perfusates into the animal's circulatory system through the heart's left ventricle, we utilized a 25 G BD Vacutainer blood collection needle (Fig. 2a). The needle is linked to a manifold fitting with stopcock, which has inlets to connect two 30 ml syringes loaded with the respective perfusates (Fig. 2b). Perfusates are injected manually by pushing the syringes. Alternatively, perfusion setups with peristaltic pumps or gravity perfusion can be used to achieve the same goal.

Hydrogel polymerization setup

For the high-temperature hydrogel polymerization step, we used a hypoxic workstation for the controlled environment of 37 °C and 0% oxygen. Alternatively, hydrogel polymerization can be done by first degassing the sample in the AP solution, covering the liquid surface with peanut oil and then incubating the polymerization reaction in a 37 °C water bath for 3 h.

3D-printed sample holder for ETC

3D-printed sample holders for ETC were printed using a conventional FDM 3D printer. The .stl model file of the ETC sample holder we designed for Logos X-CLARITY system can be found as Supplementary Software 1. For better durability of the printed assembly during ETC, use polycarbonate filament as the printing material.

3D-printed sample holder for imaging

3D-printed sample holders for sample mounting were printed using a conventional FDM 3D printer. The .stl model file of the holder we designed for Zeiss Z.1 can be found as Supplementary Software 2. For optimal results, use transparent PLA filament as the printing material.

Workstation for image analysis

A workstation with adequate central processing unit and graphics processing unit processing power is recommended for a short processing time. A large data storage capacity with fast read/write speed is necessary to handle the big data size, especially for tile-scan images of whole mouse hearts. We recommend solid-state drive-based Redundant Array of Independent Disks storage. To use Imaris for data analysis, the workstation must meet the minimum system requirement of Imaris. Images shown here were processed by a workstation with a 64-core AMD Ryzen Threadripper PRO 3995WX, 1,024 GB random access memory (RAM) and an Nvidia RTX A6000 graphics processing unit.

Procedure

Animal model preparation

● **TIMING 19–25 d, depending on model**

1. Administer intraperitoneal injections of 80 mg/kg tamoxifen to 2-week-old *Cdh5–Cre*^{ERT2}; *Rosa–LSL–tdTomato* mice daily for 5 consecutive days to induce tdTomato expression in ECs.

   ▲ **CRITICAL STEP** It is essential to consistently administer the right dose of tamoxifen over the specified period. Inadequate tamoxifen dosage or inconsistent administration may lead to insufficient tdTomato expression in ECs, affecting the downstream analysis.

   ◆ **TROUBLESHOOTING**

2. Prepare the mouse model of interest.
   (A) **Syngeneic EgfrvIII$^+$ GBM model preparation**[7]:
      (i) Inject ~8-week-old *Cdh5–Cre*^{ERT2};*Rosa–LSL–tdTomato* mice orthotopically and stereotactically with 1×10^5 mouse EgfrvIII$^+$ GBM tumor cells in a total volume of 1 µl.
      (ii) 10 d after the injection, confirm and monitor tumor growth via bioluminescence using an IVIS 200 Spectrum Imaging System after retro-orbital injection of D-luciferin.
      (iii) After administrating the treatment of interest or after the tumor has reached a certain size, e.g., 300 mm^3 usually 3 weeks after tumor induction, or estimated by bioluminescence imaging, introduce 5×10^6 mouse CAR T cells, transduced by the MMLV–139scFv–T2A–mTagBFP2–P2A–nLuc retrovirus, intravenously.
      (iv) Collect GBM tumor samples 48–72 h after CAR T injection.
      ◆ **TROUBLESHOOTING**
   (B) **Myocardial infraction model preparation**[11]:
      (i) Administer buprenorphine sustained-release (1 mg/kg) to *Cdh5–Cre*^{ERT2};*Rosa–LSL–tdTomato* mice (6–8 weeks old) 1 h before surgery, then anesthetize the mice by injecting 100 mg/kg ketamine and 10 mg/kg xylazine. Proceed with intubation and ventilation at 100 breaths per min using a rodent ventilator.
      ▲ **CRITICAL STEP** Anesthetizing mice correctly is crucial to ensure their welfare during the surgical procedure. Failure to administer the appropriate anesthetic dose could result in animal discomfort and compromise surgery outcome.
      (ii) Perform a sternotomy, then ligate the proximal left anterior descending with 8-0 Prolene thread. Verify ligation by blanching and dysfunction of the anterior wall. Maintain anesthesia during surgery with isoflurane (1–3%).
      (iii) Collect heart samples 2–3 weeks after the surgery.

Sample preparation

● **TIMING 2–3 d**

3. If samples need hypoxia staining, inject 100 µl of pimonidazole HCl (Hypoxyprobe) in saline intravenously into the mice at a 60 mg/kg concentration, 30 min before sample collection.
   ◆ **TROUBLESHOOTING**
4. If samples require conjugated-lectin perfusion imaging, inject 100 µl of DyLight 649-conjugated lectin in saline intravenously into the mice at a 55 µg/kg concentration, 5 minbefore sample collection.
   ◆ **TROUBLESHOOTING**
5. Kill the mice.
   ▲ **CAUTION** Kill the experiment animal adhering to your institution's guidelines and approved animal protocol.
   ▲ **CRITICAL STEP** Do not kill more than one mouse at a time. Transcardial perfusion steps in this protocol are postmortem. Failure to perfuse killed mice immediately will lead to blood retention in the vessels, causing high staining background and autofluorescence.
6. Immediately after killing, perform transcardial perfusion on the animal with 20 ml of the anticoagulant perfusate at a slow and steady rate (~5 ml/min) (Fig. 2a).
   ▲ **CRITICAL STEP** Outflowing perfusate should be clear by the end of this step. Repeat this step if it still contains blood.
7. Switch the perfusate to AP solution using the stopcock (Fig. 2b) and perfuse the animal with 25 ml ice-cold AP solution at a slow and steady rate (~5 ml/min).
   ▲ **CRITICAL STEP** It is critical that the perfusion process is performed slowly and at a steady rate to ensure thorough perfusion of the tissue. Failure to do so can result in uneven fixation, high staining background, high autofluorescence and potential distortion of the tissue architecture. Successful perfusion can be verified by change in the color of the heart and liver (from bright or dark red to light salmon or yellow) and stiffening of limbic muscles (Fig. 2c).
   ◆ **TROUBLESHOOTING**

8. Extract the tissue of interest. Completely submerge the tissue sample in at least 5 ml of ice-cold AP solution. Keep the sample on ice.
   ▲ **CRITICAL STEP** The extraction of tissue needs to be done quickly and carefully to prevent any cellular changes that can occur post-killing. Ensure a swift transition from the body to the AP solution.
9. Incubate the extracted tissue sample in the AP solution at 4 °C for 3 d for a mouse brain sample, or 2 d for a mouse heart sample.
   ▲ **CRITICAL STEP** The tissue must be adequately and evenly permeated by the AP solution to ensure effective preservation. Make sure the tissue is entirely immersed in the solution. As the AP solution needs to be distributed uniformly throughout the sample, the actual incubation time of this step depends on the sample volume. Incubation time of more than 3 d is not recommended, as it may lead to over-fixation and excessive cross-linking.

Hydrogel polymerization

● **TIMING 3.5 h**

10. Briefly degas the samples in AP solution using a vacuum chamber.
    ▲ **CRITICAL STEP** The presence of oxygen inhibits the polymerization reaction of the hydrogel.
    ◆ **TROUBLESHOOTING**
11. Leaving the lid or cap open to allow gas exchange, place the samples in a hypoxic workstation set to 37 °C and 0% oxygen. Alternatively, add a few drops of peanut oil to prevent gas exchange, close the lid or cap and place the samples in a 37 °C water bath.
12. Incubate samples for 3 h. Ensure the incubation conditions are strictly maintained to ensure successful polymerization. Any deviations could affect the integrity of the hydrogel.
    ▲ **CRITICAL STEP** The incubation period must be strictly controlled for successful hydrogel polymerization. Any deviations from this can affect the integrity of the hydrogel and the tissue embedded within it. Incubation time longer than 3 h may lead to excessive polymerization, making antibodies harder to penetrate in the immunostaining steps. Insufficient polymerization may lead to loss of protein during the semi-clearing steps.
    ◆ **TROUBLESHOOTING**
13. Remove samples from the hypoxia incubator chamber (Fig. 3a,b). If excessive gel formation is found surrounding the tissue samples, remove it by first extracting the samples from the gel, then rolling the samples on a piece of lens-cleaning tissue until the surface of the sample is exposed. Proceed with caution not to damage the tissue samples during gel removal. Aggressive or rough handling could compromise tissue integrity. At this point, the samples can be stored in a refrigerator at 4 °C overnight in the staining buffer.
14. Depending on the objective of the experiment, slice or section the tissue sample. GBM samples are cut into cubic pieces of ~3–4 mm in each dimension for ease of semi-clearing and staining (Fig. 3c,d). For MI samples, remove the thread for vessel ligation or trim down the thread as much as possible. Measure the length of long axis for each sample.

Tissue semi-clearing

● **TIMING 4–8 d**

15. Wash the tissue sample overnight in the staining buffer at 37 °C on an orbital shaker set to 300 rpm.
16. Perform tissue semi-clearing by either passive clearing or ETC.
    ▲ **CRITICAL STEP** This is a crucial step as it directly affects the imaging quality. Ensure the tissue-clearing process is properly done to get the most accurate imaging results.
    (A) **Passive semi-clearing:**
        (i) Place the samples in the clearing solution in a 50 ml conical tube. To clear multiple samples parallelly, five trimmed sample vials can be placed in a 50 ml conical tube to create compartments for six samples (Fig. 4a).
        (ii) Incubate at 37 °C with 300 rpm shaking on a Thermomixer C with a 50 ml tube adaptor (Fig. 4b).

(iii) The semi-clearing process should be finished after 7 d for a healthy or MI mouse heart (Fig. 4c), or 3–4 d for a trimmed mouse brain or GBM piece of 4 × 4 × 4 mm (Fig. 4d,e). The clearing reactions should be changed with fresh clearing solution every day for the first 3 d and every other day for the rest of the process.

(B) **Electrophoretic tissue semi-clearing:**

(i) Load the tissue sample into the X-CLARITY ETC System with the default single-sample holder or a 3D-printed ETC sample holder (Fig. 4f).

(ii) Set the clearing program to 37 °C, 1.2 A current and 30 rpm pump speed.

(iii) Run the clearing program for 1 d for mouse brain or GBM pieces (Fig. 4g), or 2 d for healthy or MI mouse heart (Fig. 4g). If the clearing result is not ideal, the samples can be further processed by passive clearing.

▲ **CRITICAL STEP** The current and temperature of the clearing program may be increased to accelerate the semi-clearing process but will lead to a higher risk of tissue yellowing, expanding and loss of molecules. Fragile tissues or tissues with nonhomogenous textures that may expand at different rates, such as MI heart samples, may be damaged by ETC. For these samples, passive semi-clearing is recommended.

◆ **TROUBLESHOOTING**

17. Wash the cleared tissue sample in the staining solution at 37 °C on a shaker overnight.

■ **PAUSE POINT** At this point, the tissue sample can be stored in the staining solution at 4 °C for at least 2 months.

Immunostaining

● **TIMING 3–6 d**

18. Place the tissue samples in the staining buffer with primary antibody (starting at 20 µg/ml). For small mouse brains or GBM pieces, place one sample per well in a 96-well plate, add 200 µl staining solution to each well, then seal the 96-well plate with a PCR plate sealing sticker. For mouse hearts, incubate the sample in a 1.5 ml tube with >500 µl staining solution. For samples with a high presence of cells expressing Fc receptors, such as mouse GBM tumor, add 20 µg/ml TruStain FcX anti-mouse CD16/32 antibody to the staining buffer along with the primary antibodies to reduce the staining background.

▲ **CRITICAL STEP** 20 µg/ml is generally a good starting point for testing an unknown antibody for LSFM application. A high concentration of antibodies is crucial for effective penetration and sufficient binding to epitopes. For staining immune cells, we recommend testing the antibody viability by including a positive control tissue (e.g., a slice of mouse spleen) that was processed the same way as your tissue of interest.

For a combinational immunostaining, e.g., unconjugated primary + conjugated secondary antibodies on antigen A and conjugated primary antibody on antigen B, incubate the conjugated primary antibody on antigen B with the conjugated secondary antibody on antigen A.

For a list of antibodies used in the samples shown here, see Table 1.

◆ **TROUBLESHOOTING**

19. Incubate the samples in the staining solution at 37 °C with 300 rpm orbital shaking for 1 d.

▲ **CRITICAL STEP** For larger samples with high epitope abundance, spiking in fresh primary antibodies may be necessary as the antibody in the staining buffer may be depleted.

20. Incubate the samples in the staining solution at 4 °C with 300 rpm orbital shaking for 12 h.

21. Incubate the samples in the staining solution at room temperature with 300 rpm orbital shaking for 12 h.

22. Wash the staining samples in a deep 96-well plate with 1.5 ml staining buffer in each well. Seal the 96-well plate with a PCR plate sealing sticker. Incubate the samples at 37 °C with 300 rpm orbital shaking for 1 d.

23. If staining of secondary antibodies is needed, repeat Steps 18–22 with your secondary antibodies of choice in place of primary antibodies.

RI matching and sample mounting

● **TIMING 12–24 h**

24. Incubate the tissue sample in RIMS at 37 °C with 300 rpm orbital shaking for 12–24 h, based on the sample volume. After the incubation, measure the length of the long axis for each sample (Fig. 5a–c).
    ▲ **CRITICAL STEP** RIMS buffer usually has a higher density compared with the sample, which will stay afloat in RIMS in this step and not completely immersed, leading to inconsistent RI throughout the sample. Fill the whole sample container with RIMS to avoid this. If the sample volume is large, staining buffer in the sample may dilute the RIMS buffer, leading to a decrease in RI. RIMS may be refreshed after 8 h to ensure a big RI-matched sample has an RI closer to 1.46.
    ◆ **TROUBLESHOOTING**
25. Cut off the front end of a 3 ml syringe and pull back the plunger. Keep the syringe upside down and add 1 ml of warm RIMS–agar solution into the syringe (Fig. 5d). Keep the rest of the RIMS–agar solution on a heating block at 50 °C. Wait ~10 min for the RIMS–agar solution to cool below the gel point and solidify.
26. Carefully drop the RI-match sample on top of the solidified bottom gel layer.
27. Add RIMS–agar solution enough to cover the whole sample. Wait ~10 min for the RIMS–agar solution to cool below the gel point and solidify.
28. If the sample floats to the top before solidification and is partly exposed, add more warm RIMS–agar solution to the top to encapsulate the whole sample.
29. After the agar block has solidified (Fig. 5d), push the block out using the plunger.
30. Carefully trim down the excessive agar and remove all curved edges (Fig. 5e).
31. Use cyanoacrylate glue to fix the agar block to a 3D-printed sample holder (Fig. 5f).
    ◆ **TROUBLESHOOTING**
32. Keep the mounted sample in RIMS until imaging (Fig. 5g).
    ■ **PAUSE POINT** After the samples are mounted in RIMS, you may store the samples in RIMS at 4 °C for at least 1 week until you are ready to proceed with imaging. Warm up the sample in RIMS to room temperature before imaging, as temperature can affect the RI.

Sample imaging

● **TIMING 10–30 min per sample**

33. Turn on the Zeiss Z.1 microscope and the workstation. Start the ZEN software and initialize the microscope.
34. Fill the sample chamber with ~20 ml RIMS.
35. Mount the sample holder with the sample mounted in Step 31. Insert the RIMS-filled sample chamber into the microscope.
36. Locate the sample using the sample positioning camera. Rotate and move along the *x*–*y* plane to acquire a desired view of the sample.
37. Turn on the 561 nm laser and use an LP 585 filter set to observe the tdTomato signal. Use its emission to find the focus and ROI in the sample.
    ◆ **TROUBLESHOOTING**
38. Activate pivot scanning mode to reduce stripe bands on the image created by bubbles or debris. Set desired acquisition dimension and zoom. Based on the fluorophore present in the sample, set the filter set, laser intensity and exposure time for each acquisition track. These settings should stay unchanged for all samples of the same experiment.
39. Define a *Z*-stack that covers the whole ROI. The thickness of the light sheet can be adjusted for a better *z*-axis resolution. For a 4 × 4 × 4 mm mouse brain or GBM piece, a typical 2 × 2 mm *x*–*y* acquisition area and a >2 mm *z*-axis depth is used. Tile-scan parameters will need to be set up for imaging a whole mouse healthy or MI heart.
    ◆ **TROUBLESHOOTING**
40. Acquire the image and properly save the data for downstream processing.
    ▲ **CRITICAL STEP** Be sure to properly save and organize the image data. Mismanaged data can lead to confusion and mistakes in the subsequent analysis stages.

■ **PAUSE POINT** Imaged samples in RIMS can be stored long term at 4 °C with no light exposure for re-imaging in the future. The length of the maximum storage time depends on tissue type and fluorophore stability. tdTomato and other fluorophores in mouse GBM sample and mouse heart sample are stable for at least 2.5 years (Extended Data Fig. 2).

Image processing and analysis

● **TIMING 0.5–2 h per sample**

41. Convert raw .czi files to .ims files using Imaris Converter. For tile-scan images, the tiles are stitched using Imaris Stitcher and saved as single .ims files. Open the image in Imaris 10. Figure 11 show an overview of the image processing and analysis workflow.
42. If precise structural dimensions are crucial to the downstream analysis, readjust the voxel size in 'Image Properties' by a single factor calculated from the sample long-axis length measured before tissue semi-clearing and after RI matching to correct the sample expansion or shrinkage (Extended Data Fig. 3a).
    ◆ **TROUBLESHOOTING**
43. Use 'Crop 3D' to crop out the ROI. The selection of ROI aims at excluding all nontumor areas for mouse GBM samples or focusing on the MI area in the left ventricle for mouse MI heart samples. The dimension of the images is standardized for all samples for generating statistics. 1 × 1 × 1 mm is typically used for GBM or brain tissue pieces, or 2 × 2 × 2 mm for LV or MI area in healthy or MI heart (Extended Data Fig. 3b).
44. In the 'Image Processing' module (Extended Data Fig. 3c), deconvolute each channel using the correct objective lens NA, medium and specimen RI, and emission wavelength (Extended Data Fig. 3d).
45. If the average intensity along the *z* axis is nonuniform due to tissue coloring or inconsistent laser illumination, the 'Normalize Layers' function can be used to correct the depth attenuation (Extended Data Fig. 3e).
46. If the sample presents a great amount of background or autofluorescence, use the 'Background Subtraction' function to reduce the background. The setting of the filter size depends on the expected size of the feature of interest (Extended Data Fig. 3e).
    ◆ **TROUBLESHOOTING**
47. For samples with injected conjugated lectin, use the 'Coloc' module to calculate and visualize the colocalization of tdTomato$^+$ vasculature and lectin-labeled perfused vasculature.
48. Create objects for feature registration and computing statistics (Fig. 11, surface, filament and spot objects, and Extended Data Fig. 3f).
    (A) **Global features used as a volumetric normalizing factor (e.g., GBM cell expressed GFP, tissue autofluorescence in mouse heart)**
    (i) Use the 'Add new Surfaces' function on the channel of tumor cell-specific signal for GBM samples (Figs. 7 and 8, GFP$^+$ tumor cells panels) or tdTomato channel for healthy or MI heart sample boundary (Fig. 6, cyan surface volume object, when using a low threshold).
    (ii) Set the width parameter for 'Smooth' and use 'Absolute Intensity' as the thresholding method (Extended Data Fig. 3g).
    ▲ **CRITICAL STEP** The smoothing factor, or width, is crucial in correctly approximate feature boundary. The exact value should be dependent on the nature of the feature being analyzed. A width of 3–4 voxels is recommended for small features with structure details. A bigger width can be used when approximating the boundary of tissue or tumor.
    (iii) The threshold of the surface object should be set to a level low enough to clearly define the feature boundary and high enough to not include any background noise (Extended Data Fig. 3h).
    (iv) Filter the generated objects by size (e.g., number of voxels, volume or bounding box length) to remove any tiny objects of only a few voxels that are caused by random noise or impurities in the mounting RIMS–agar gel (Extended Data Fig. 3i).
    (v) Export the statistics of generated surface objects as .csv files.

(B) **Vascular features (e.g., tdTomato$^+$ vasculature, conjugated lectin perfusion, colocalization of tdTomato and conjugated lectin for perfused vessel)**

(i) Use the 'Add new Filaments' function on the vasculature-related channel. For detection type, use the Autopatch algorithm with no soma or spine. Include object–object statistics.

(ii) Use 'Multiscale Points' to generate seed points (Extended Data Fig. 3j). For the thinnest/largest diameters, provide an approximation by viewing the whole *Z*-stack using the Slicer rendering and measuring the thinnest and the thickest point in the vascular network. Choose an appropriate seed point threshold that visually denotes all vascular segments but not noise or isolated spots or volumes in the tissue (Extended Data Fig. 3k).

(iii) For the 'Segment Classification' step, use the pointer and circle selection tools to select the generated segments and assign them to the Keep (correctly recognized segments) or Discard (misrecognized segments) training set. Ideally, each set should have ~50 segments to provide a robust predictive classification (Extended Data Fig. 3l).

(iv) Hit 'Train and Predict' to predict the kept and discarded segments using machine learning-based models generated from the training set defined in the last step.

(v) Export the statistics of generated filament objects as .csv files.

◆ **TROUBLESHOOTING**

(C) **Spot features (e.g., mTagBFP2$^+$ CAR T cells, immune cell surface markers)**

(i) Use the 'Add new Spots' function on the immune cell-related channels. Include object–object statistics and the 'Different Spot Sizes' setting (Extended Data Fig. 3m).

(ii) An appropriate *XY* diameter for the single cells with a specific signal is needed to correctly count and locate the cells if they are present in clusters. Measure the diameter of a single-cell signal using the slicer rendering to generate seed points. Alternatively, assume the regular diameter of the feature (e.g., the diameter of mouse T cells) if sample deformation has been corrected (Extended Data Fig. 3n).

(iii) Filter the generated spot seed points by quality to exclude the low-signal, high-noise events (Extended Data Fig. 3o).

(iv) Set appropriate threshold for the spot objects to make sure the boundary covers the diameter of the features (Extended Data Fig. 3o).

(v) Export the 'Average Values' and the 'Specific Values' statistics of generated spot objects as .csv files.

◆ **TROUBLESHOOTING**

49. Calculate the sample or object-specific criteria using the exported statistics (Fig. 9).

▲ **CRITICAL STEP** Check the image processing and feature registration settings for each sample and make sure they are consistent across all samples within a single experiment to ensure data integrity and comparability.

Troubleshooting

Troubleshooting advice can be found in Table 2.

Table 2 | Troubleshooting table

Step	Problem	Possible reason	Solution
1	Inadequate tdTomato expression in ECs	Inconsistent administration or inadequate dosage of tamoxifen	Ensure consistent administration of tamoxifen sufficient to induce tdTomato expression in ECs. Inaccurate dosing or inconsistent administration may result in insufficient tdTomato expression, affecting the downstream analysis
2A	Unable to visualize CAR T cell delivery to the tumor	Ineffective retroviral transduction	Optimize retroviral transduction efficiency of mouse CAR T cells

Table 2 (continued) | Troubleshooting table

Step	Problem	Possible reason	Solution
		Improper injection	Ensure accurate and timely intravenous injection of 5×10^6 transduced CAR T cells into the mice
		Tumor samples are too thick for a good penetrance of 405 nm excitation light (for mTagBFP2-based detection in vitro)	Trim the sample to make it thinner, or use a different way of labeling CAR T cells (by other fluorescent reporter, such as GFP, or by immunostaining with a CAR-specific antibody)
3	Poor or inconsistent hypoxia staining	Improper injection or concentration of pimonidazole HCL	Ensure accurate injection of pimonidazole HCL at the correct concentration
			Verify the timing of the injection to allow sufficient time for distribution in the tissue
4	Inadequate lectin perfusion or staining	Incorrect injection technique or concentration of conjugated lectin	Verify the injection technique and ensure an accurate concentration of the lectin solution
			Adjust the timing to allow proper perfusion
7	High blood retention in vasculature resulted in autofluorescence	Inadequate perfusion of anticoagulant and ice-cold AP solution	Ensure a slow and steady perfusion rate to effectively distribute the anticoagulant perfusate and ice-cold AP solution throughout the animal's circulation
		Insufficient perfusion rate or perfusate did not fully enter the body circulation	Pay careful attention to the perfusion technique to achieve thorough and uniform perfusion. Minimize premature tissue fixation by keeping the AP solution on ice
10, 12	Loss of biomolecules or tissue integrity due to insufficient hydrogel polymerization	Inadequate vacuum, sealing	Degas the samples in AP solution for longer before proceeding with hydrogel polymerization to make sure that air in the solution is removed
			Ensure proper sealing of the samples to prevent gas exchange that may interfere with the polymerization process
		Incorrect temperature or oxygen levels	If using a hypoxia workstation, start the polymerization process only after the environment has met the set points. Maintain strict adherence to the specified incubation conditions of 37 °C and 0% oxygen to ensure successful hydrogel polymerization
16	Insufficient tissue clearing	Incorrect shaking speed, temperature or clearing solution	Use the appropriate shaking speed, maintain the correct temperature, and refresh the clearing solution as prescribed
		Insufficient clearing due to big tissue volume	In the case of unsatisfactory results, consider extending the clearing time or trimming the sample
16A	Tissue damage, yellowing, or irreversibly expanded during ETC	Sample expose to high current or temperature	Lower current and temperature setting for a mild ETC of longer duration. An ETC-passive clearing combination can be used for an optimal clearing result
18	Uneven or absent staining	Low-quality or incorrect antibody concentration	Ensure the use of high-quality antibodies and verify the appropriate concentration for optimal staining results
			Maintain the correct shaking speed and temperature during the staining process
			Review the antibody selection and titration process if staining quality is consistently poor
		Excessive cross-linking within tissue	Consider lowering acrylamide or PFA concentration in the AP solution for a better antibody penetration
24	Agar solution does not solidify	Temperature of the agar solution not cooled sufficiently	If the agar solution fails to solidify, confirm that the temperature is appropriately cooled
			Adjust the cooling time if necessary to achieve proper gel formation
31	Sample or RIMS–agar encapsulated sample does not stick to sample holder	Too much glue applied	Apply only a thin layer of glue on the sample holder
		Too much RIMS residue on the contact surface	Remove excessive RIMS on the sample or agar block before placing it on the applied glue layer
37	Difficulty focusing on the tdTomato signal	Incorrect laser settings or filter set	Verify that the correct laser intensity, filter set, and exposure time are set for the tdTomato fluorophore
			Adjust the focus and imaging parameters to optimize visualization of the tdTomato signal
39	GBM tumor sample has red/black coloring that blocks illumination or emission	Bleeding or necrotic area at tumor core	Severe tumor has bleeding or necrotic area at the tumor area that cannot be eliminated by perfusion. Consider reducing depth of *Z*-stack or trim the sample to make it thinner to minimize the effect
40	RIMS buffer creates a shimmering 'wave' effect around and on top of ROI	Glue reacted with histodenz, creating precipitation and inconsistent RI	Apply only a minimal amount of glue when mounting samples
			Filter and homogenize 'glue-contaminated' RIMS. Measure RI and spike in histodenz if RI reduction is observed. Measure RI and adjust deviation by adding water, evaporating or spiking in histodenz if RI increase or reduction is observed, respectively

Table 2 (continued) | Troubleshooting table

Step	Problem	Possible reason	Solution
42	Sample voxel size disproportionally warped on the three axes	Sample expansion or shrinkage during tissue semi-clearing and RI matching was nonisotropic	Samples with fibrous texture or sample semi-clearing by ETC with a sample holder too small may have nonisotropic change in sample volume. Measuring and recording changes on all axes is needed to correct each axis separately
46	Excessive background or autofluorescence after image processing	Inappropriate setting for 'Background Subtraction' filter size	Adjust the filter size based on the expected size of the feature of interest; use a bigger value for a globally present background
		Laser intensity is too high, or exposure time is too long	Review imaging settings and acquisition parameters to minimize autofluorescence and optimize signal-to-noise ratio
		Nonspecific expression of fluorescent reporter protein	Review genotype and phenotype of the animal model being used; inspect a thin slice of a fresh tissue sample with an epi-fluorescence microscope before moving to the tissue processing steps
48B	Incorrect detection of vascular features	Inadequate seed points or misrecognized segments during training and prediction	Adjust the *XY* diameter for seed points to accurately locate vascular segments
			Reevaluate the training process, including segment selection and assignment, and review the classification model. Ensure an appropriate sample size for training to improve the detection of vascular features. Increase the sample size of training segments to provide a more robust training set. Ensure proper selection and assignment of segments as 'Keep' or 'Discard' during the training step
48C	Incorrect detection of spot features	Inadequate spot diameter or low signal-to-noise ratio	Adjust the spot diameter based on the size of the feature of interest
			Filter the spot objects by quality to exclude low-signal, high-noise events
			Review the imaging settings and acquisition parameters to enhance the signal-to-noise ratio of the spot features

Timing

Step 1, tamoxifen induction of tdTomato expression in ECs: 5 d
Step 2, animal model preparation:
Option A: syngeneic EgfrvIII^{+} GBM model: 14 d
Option B: myocardial infraction model: 14–21 d
Steps 3–9, sample preparation: 2–3 d
Steps 10–14, hydrogel polymerization: 3.5 h
Step 15, AP solution removal: 18 h
Step 16, tissue semi-clearing:
Option A: electrophoretic tissue semi-clearing: 1–2 d
Option B: passive tissue semi-clearing: 3–7 d
Step 17, clearing solution removal: 18 h
Steps 18–23, immunostaining: 3–6 d
Steps 24–32, RI matching and sample mounting: 12–24 h
Steps 33–40, sample imaging: 10–30 min
Steps 41–49, image processing and analysis: 0.5–2 h

Anticipated results

We present an optimized protocol for the comprehensive analysis of spatiotemporal regulations within tissue microenvironments, with a specific emphasis on vasculature and immune cells. Successful implementation of this protocol facilitates a robust comprehension of the implications of these microenvironmental components in disease progression and therapeutic responses, particularly in the domains of cancer and CVD. When executed appropriately, this protocol yields high-resolution LSFM images of entire tissue samples, offering a high level of detail and precision compared with conventional thin-tissue slide

imaging. Notably, these images provide clear visualization of tissue vasculature and immune components, as exemplified in Figs. 6–8.

Figure 6 illustrates LSFM images of vasculature and its perfusion in healthy and ischemic heart tissues, in which fluorescence dye-conjugated lectin was infused. Using this protocol, our previous investigation revealed that the vasculature within the MI region, despite its robust presence, exhibited inadequate perfusion and a disorganized arrangement, lacking a distinct vascular hierarchy (Fig. 6, right).

Figures 7 and 8 showcase LSFM images of normal brain and tumor tissues. By employing lectin perfusion in conjunction with tdTomato-labeled vasculature, nonproductive, abnormal angiogenesis in the tumor microenvironment can be identified (Fig. 7a). Moreover, hypoxyprobe immunostaining allows for visualization of spatially heterogeneous hypoxic areas within the tumor (Fig. 7b), providing additional resolution of vascular functions in the tumor microenvironment. Additionally, these images also demonstrate discernable signals of GFP expression by GBM tumor cells, indicating tumor volume and boundaries. Furthermore, when tumor-bearing mice are treated with fluorescent reporter-labeled CAR T cells, collected samples can be imaged to assess CAR T cell infiltration (Fig. 8a). The integration of such samples with CD3ε and CD8a staining enables the examination of the composition and spatial distribution of immune components within the tumor (Fig. 8b).

Figures 9 and 10 provide an in-depth analysis of various factors related to tumor vascularity and immunity. Specifically, vascular perfusion with DyLight 649–lectin was visualized in tumor with spatially distributed vascular diameters and volumes calculated (Fig. 9a–c). We quantified the vessel leakage within the tumor region, depending on a comparison between the volumes of tdTomato and lectin signals (Fig. 9d,e). The analysis of the border zone of MI cardiac tissues depicts the tissue boundary and perfused areas, with the portion of nonperfused, ischemic area calculated accordingly (Fig. 9f,g). Furthermore, the distance of mTagBFP2$^+$ CAR T cells to their closest tdTomato$^+$ blood vessels provide insights into the spatial regulation of immune cells near the tumor vasculature (Fig. 10a). Finally, the feature analysis of infiltrating T cells based on immunostained markers shows the subtype composition of CD3$^+$ cells and their spatial relationships (Fig. 10b–d). These quantitative analyses complement the visual insights from the LSFM images, providing a thorough, robust understanding of the vascular and immune landscapes within the tissues.

This protocol has been optimized to ensure a high degree of reproducibility and cost effectiveness (Fig. 11), thus enhancing its accessibility for a wide range of biological laboratories. The techniques described herein prioritize the preservation of endogenous fluorescent reporters and immune antigens, thereby guaranteeing the collection of high-quality and reliable data. Successful implementation of this protocol will provide critical information about spatial regulation of tissue vascularization and immunity, promising in-depth investigations into disease progression, potentially leading to breakthroughs in novel therapeutic strategies for cancer and CVD. By advancing our understanding of the influence exerted by vascular structure and immune cell composition on disease progression, researchers will be empowered to design and implement innovative interventions for the treatment of these conditions.

Reporting summary

Further information on research design is available in the Nature Portfolio Reporting Summary linked to this article.

Data availability

The main data discussed in this protocol are available in the supporting primary research papers[7,8,11]. The raw datasets of the main data and of the additional new data shown in this work are available for research purposes from the corresponding authors upon reasonable request.

Received: 31 May 2023; Accepted: 25 October 2023;
Published online: 11 January 2024

References

1. Anderson, N. M. & Simon, M. C. The tumor microenvironment. *Curr. Biol.* **30**, R921–R925 (2020).
2. Binnewies, M. et al. Understanding the tumor immune microenvironment (TIME) for effective therapy. *Nat. Med.* **24**, 541–550 (2018).
3. Sun, K., Li, Y. Y. & Jin, J. A double-edged sword of immuno-microenvironment in cardiac homeostasis and injury repair. *Signal Transduct. Target Ther.* **6**, 79 (2021).
4. Jain, R. K. et al. Angiogenesis in brain tumours. *Nat. Rev. Neurosci.* **8**, 610–622 (2007).
5. Jain, R. K. Normalization of tumor vasculature: an emerging concept in antiangiogenic therapy. *Science* **307**, 58–62 (2005).
6. Lamplugh, Z. & Fan, Y. Vascular microenvironment, tumor immunity and immunotherapy. *Front. Immunol.* **12**, 811485 (2021).
7. Zhang, D. et al. PHGDH-mediated endothelial metabolism drives glioblastoma resistance to chimeric antigen receptor T cell immunotherapy. *Cell Metab.* **35**, 517–534 e518 (2023).
8. Ma, W. et al. Targeting PAK4 to reprogram the vascular microenvironment and improve CAR-T immunotherapy for glioblastoma. *Nat. Cancer* **2**, 83–97 (2021).
9. Wu, X., Reboll, M. R., Korf-Klingebiel, M. & Wollert, K. C. Angiogenesis after acute myocardial infarction. *Cardiovasc Res.* **117**, 1257–1273 (2021).
10. Harada, K. et al. Vascular endothelial growth factor administration in chronic myocardial ischemia. *Am. J. Physiol.* **270**, H1791–H1802 (1996).
11. Huang, M. et al. Endothelial plasticity drives aberrant vascularization and impedes cardiac repair after myocardial infarction. *Nat. Cardiovasc. Res.* **1**, 372–388 (2022).
12. Ntziachristos, V. Going deeper than microscopy: the optical imaging frontier in biology. *Nat. Methods* **7**, 603–614 (2010).
13. Huisken, J., Swoger, J., Del Bene, F., Wittbrodt, J. & Stelzer, E. H. Optical sectioning deep inside live embryos by selective plane illumination microscopy. *Science* **305**, 1007–1009 (2004).
14. Renier, N. et al. IDISCO: a simple, rapid method to immunolabel large tissue samples for volume imaging. *Cell* **159**, 896–910 (2014).
15. Cai, R. et al. Panoptic imaging of transparent mice reveals whole-body neuronal projections and skull–meninges connections. *Nat. Neurosci.* **22**, 317–327 (2019).
16. Qi, Y. et al. FDISCO: advanced solvent-based clearing method for imaging whole organs. *Sci. Adv.* **5**, eaau8355 (2019).
17. Hahn, C. et al. High-resolution imaging of fluorescent whole mouse brains using stabilised organic media (sDISCO). *J. Biophotonics* https://doi.org/10.1002/jbio.201800368 (2019).
18. Pan, C. et al. Shrinkage-mediated imaging of entire organs and organisms using uDISCO. *Nat. Methods* **13**, 859–867 (2016).
19. Tainaka, K. et al. Chemical landscape for tissue clearing based on hydrophilic reagents. *Cell Rep.* **24**, 2196–2210.e2199 (2018).
20. Tainaka, K., Kuno, A., Kubota, S. I., Murakami, T. & Ueda, H. R. Chemical principles in tissue clearing and staining protocols for whole-body cell profiling. *Annu. Rev. Cell. Dev. Biol.* **32**, 713–741 (2016).
21. Tainaka, K. et al. Whole-body imaging with single-cell resolution by tissue decolorization. *Cell* **159**, 911–924 (2014).
22. Murakami, T. C. et al. A three-dimensional single-cell-resolution whole-brain atlas using CUBIC-X expansion microscopy and tissue clearing. *Nat. Neurosci.* **21**, 625–637 (2018).
23. Susaki, E. A. et al. Advanced CUBIC protocols for whole-brain and whole-body clearing and imaging. *Nat. Protoc.* **10**, 1709–1727 (2015).
24. Hama, H. et al. ScaleS: an optical clearing palette for biological imaging. *Nat. Neurosci.* **18**, 1518–1529 (2015).
25. Hama, H. et al. Scale: a chemical approach for fluorescence imaging and reconstruction of transparent mouse brain. *Nat. Neurosci.* **14**, 1481–1488 (2011).
26. Chung, K. et al. Structural and molecular interrogation of intact biological systems. *Nature* **497**, 332–337 (2013).
27. Yang, B. et al. Single-cell phenotyping within transparent intact tissue through whole-body clearing. *Cell* **158**, 945–958 (2014).
28. Richardson, D. S. et al. Tissue clearing. *Nat. Rev. Methods Primers* https://doi.org/10.1038/s43586-021-00080-9 (2021).
29. Richardson, D. S. & Lichtman, J. W. Clarifying tissue clearing. *Cell* **162**, 246–257 (2015).
30. Wang, Y. et al. Ephrin-B2 controls VEGF-induced angiogenesis and lymphangiogenesis. *Nature* **465**, 483–486 (2010).
31. Ranchoux, B. et al. Endothelial-to-mesenchymal transition in pulmonary hypertension. *Circulation* **131**, 1006–1018 (2015).
32. Huang, M. et al. c-Met-mediated endothelial plasticity drives aberrant vascularization and chemoresistance in glioblastoma. *J. Clin. Invest.* **126**, 1801–1814 (2016).
33. Kisanuki, Y. Y. et al. Tie2–Cre transgenic mice: a new model for endothelial cell-lineage analysis in vivo. *Dev. Biol.* **230**, 230–242 (2001).
34. De Palma, M. et al. Tie2 identifies a hematopoietic lineage of proangiogenic monocytes required for tumor vessel formation and a mesenchymal population of pericyte progenitors. *Cancer Cell* **8**, 211–226 (2005).
35. Shaner, N. C. et al. Improved monomeric red, orange and yellow fluorescent proteins derived from Discosoma sp. red fluorescent protein. *Nat. Biotechnol.* **22**, 1567–1572 (2004).
36. Cormack, B. P., Valdivia, R. H. & Falkow, S. FACS-optimized mutants of the green fluorescent protein (GFP). *Gene* **173**, 33–38 (1996).
37. Renier, N. et al. Mapping of brain activity by automated volume analysis of immediate early genes. *Cell* **165**, 1789–1802 (2016).
38. Dodt, H. U. et al. Ultramicroscopy: three-dimensional visualization of neuronal networks in the whole mouse brain. *Nat. Methods* **4**, 331–336 (2007).
39. Hutchinson, M. H., Dorgan, J. R., Knauss, D. M. & Hait, S. B. Optical properties of polylactides. *J. Polym. Environ.* **14**, 119–124 (2006).
40. Eliat, F. et al. Tissue clearing may alter emission and absorption properties of common fluorophores. *Sci. Rep.* **12**, 5551 (2022).

Acknowledgements
This work was supported in part by National Institutes of Health grants R01NS094533 (to Y.F.), R01NS106108 (to Y.F.), R01CA241501 (to J.F.D. and Y.F.) and R01HL155198 (to Y.G. and Y.F.), and by American Heart Association grants Innovative Project Award (to Y.F.), Transformational Project Award (to Y.G.) and Predoctoral Fellowship (to D.Z.).

Author contributions
D.Z. and Y.F. initiated the project. D.Z. performed most of the experiments and originally developed the protocol. D.Z., A.H.C., E.K., K.H., A.L.S. and J.F.D. designed the experiments. D.Z., C.Y. and W.Z. contributed to imaging analysis. Y.G. and Y.F. supervised the project. D.Z., E.K. and Y.F. wrote the manuscript. All authors commented on the manuscript.

Competing interests
The authors declare no competing interests.

Additional information
Extended data is available for this paper at https://doi.org/10.1038/s41596-023-00941-5.

Supplementary information The online version contains supplementary material available at https://doi.org/10.1038/s41596-023-00941-5.

Correspondence and requests for materials should be addressed to Yanqing Gong or Yi Fan.

Peer review information *Nature Protocols* thanks Hiroki Ueda and the other, anonymous, reviewer(s) for their contribution to the peer review of this work.

Related links
Key references using this protocol
Wang, Q. et al. *Nat. Commun.* **9**, 559 (2018): https://doi.org/10.1038/s41467-018-03050-0
Ma, W. et al. *Nat. Cancer* **2**, 83–97 (2021): https://doi.org/10.1038/s43018-020-00147-8
Huang, M. et al. *Nat. Cardiovasc. Res.* **1**, 372–388 (2022): https://doi.org/10.1038/s44161-022-00047-3
Zhang, D. et al. *Cell Metab.* **35**, 517–534 (2023): https://doi.org/10.1016/j.cmet.2023.01.010

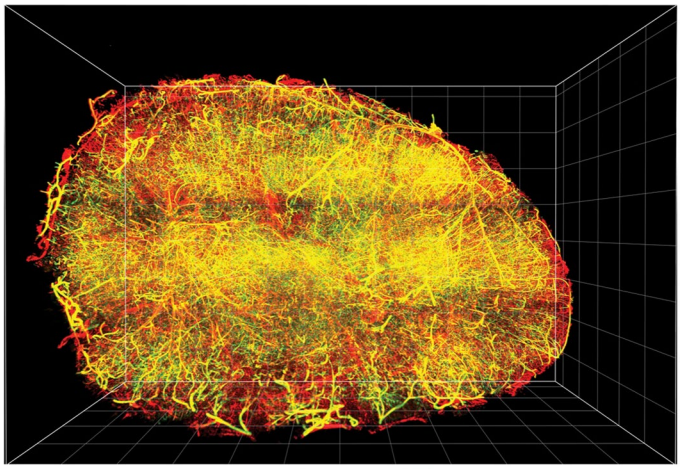

Extended Data Fig. 1 | LSFM analysis of healthy mouse brain left hemisphere. Healthy *Cdh5-Cre*^{ERT2};*LSL-tdTomato* mice were perfused with DyLight 649-lectin. Brain tissue was excised, followed by tissue clearing and LSFM imaging. Each minor tick on the grid represents 1 mm.

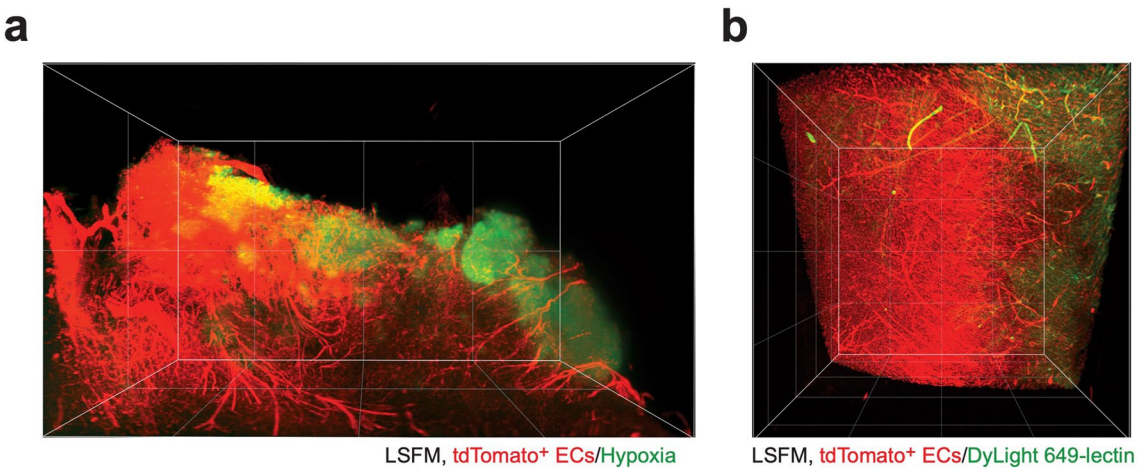

Extended Data Fig. 2 | LSFM analysis of tissue samples after long-term storage. a, GBM was induced in *Cdh5-Cre*^{ERT2};*LSL-tdTomato* mice, followed by perfused with hypoxyprobe. Tissue samples were subjected to tissue clearing, and stored in RIMS at 4°C for 2.5 years and imaged by LSFM. Each minor tick on the grid represents 1 mm. **b**, MI was induced in *Cdh5-Cre*^{ERT2};*LSL-tdTomato* mice, followed by perfused with lectin. Tissue samples were subjected to tissue clearing, and stored in RIMS at 4°C for 2.5 years and imaged by LSFM. Each minor tick on the grid represents 0.5 mm.

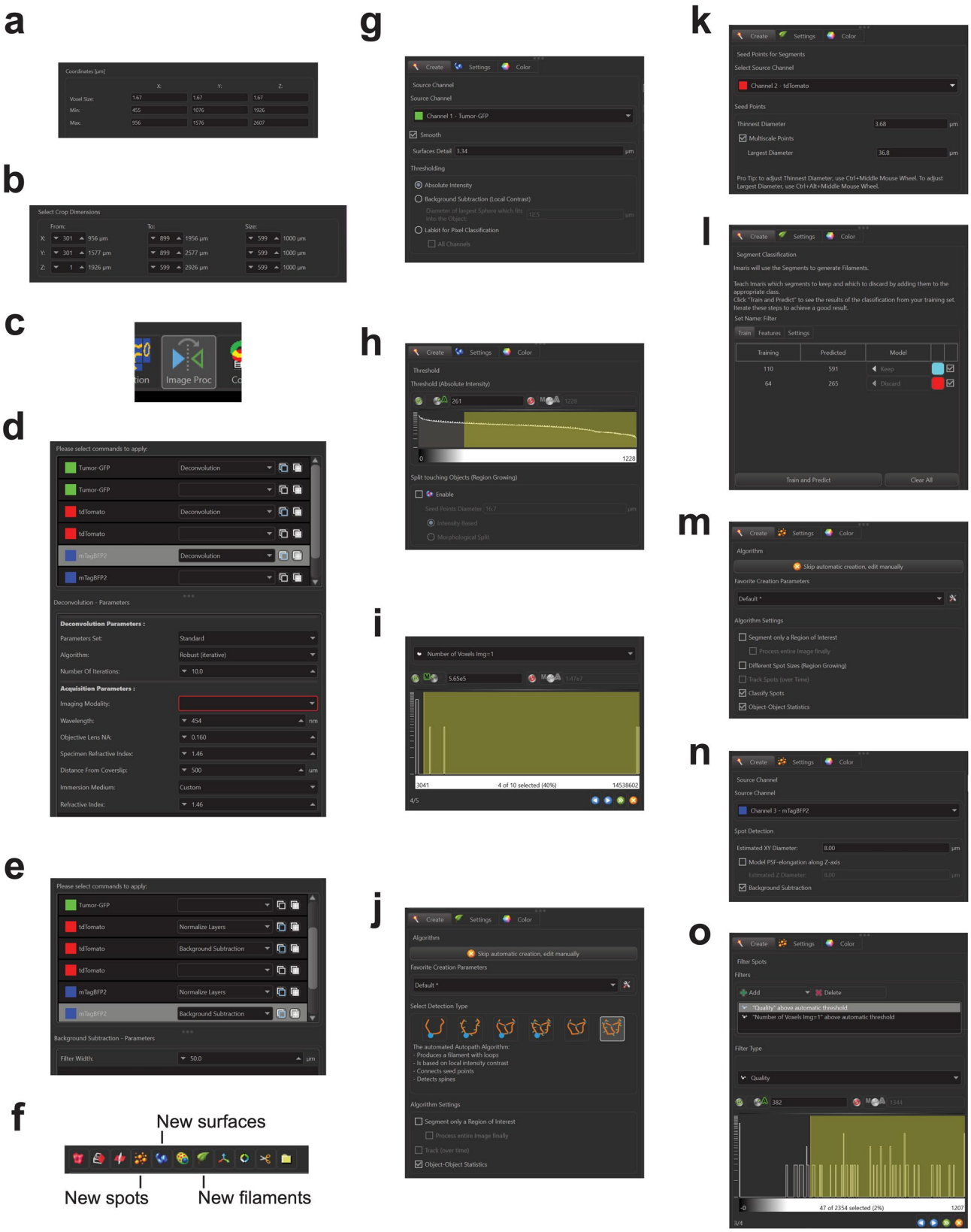

Extended Data Fig. 3 | See next page for caption.

Extended Data Fig. 3 | Key steps of image processing and analysis in Imaris. a, Voxel size correction in "Image Properties" (Step 42). **b**, Crop out ROI in "Crop 3D" (Step 43). **c**, "Image Processing" module (Step 44). **d**, Setting deconvolution parameters in the "Image Processing" module (Step 44). **e**, Preprocessing the image using "Normalize Layers" and "Background Subtraction " (Steps 45, 46). **f**, Creating objects for feature registration (Step 48). **g**, Initial parameters for creating surface objects (Step 48A(ii)). **h**, Thresholding of surface object creation (Step 48A(iii)). **i**, Filtering generated surface objects by size (Step 48A(iv)). **j**, Multiscale Points method of generating filament seed points (Step 48B(ii)). **k**, Seed point filtering by vessel diameter (Step 48B(ii)). **l**, Segment classification and filtering by machine learning-based model (Step 48B(iii)). **m**, Initial parameters for creating spot objects (Step 48C(i)). **n**, Spot detection by feature diameter (Step 48C(ii)). **o**, Filter Spot feature by quality and diameter/size (Step 48C(iii–iv)).

nature research

Corresponding author(s): Yi Fan, Yanqing Gong

Last updated by author(s): 2023-09-14

Reporting Summary

Nature Research wishes to improve the reproducibility of the work that we publish. This form provides structure for consistency and transparency in reporting. For further information on Nature Research policies, see our Editorial Policies and the Editorial Policy Checklist.

Please do not complete any field with "not applicable" or n/a. Refer to the help text for what text to use if an item is not relevant to your study.
For final submission: please carefully check your responses for accuracy; you will not be able to make changes later.

Statistics

For all statistical analyses, confirm that the following items are present in the figure legend, table legend, main text, or Methods section.

n/a Confirmed

- The exact sample size (*n*) for each experimental group/condition, given as a discrete number and unit of measurement
- A statement on whether measurements were taken from distinct samples or whether the same sample was measured repeatedly
- The statistical test(s) used AND whether they are one- or two-sided
  Only common tests should be described solely by name; describe more complex techniques in the Methods section.
- A description of all covariates tested
- A description of any assumptions or corrections, such as tests of normality and adjustment for multiple comparisons
- A full description of the statistical parameters including central tendency (e.g. means) or other basic estimates (e.g. regression coefficient) AND variation (e.g. standard deviation) or associated estimates of uncertainty (e.g. confidence intervals)
- For null hypothesis testing, the test statistic (e.g. *F*, *t*, *r*) with confidence intervals, effect sizes, degrees of freedom and *P* value noted
  Give P values as exact values whenever suitable.
- For Bayesian analysis, information on the choice of priors and Markov chain Monte Carlo settings
- For hierarchical and complex designs, identification of the appropriate level for tests and full reporting of outcomes
- Estimates of effect sizes (e.g. Cohen's *d*, Pearson's *r*), indicating how they were calculated

Our web collection on statistics for biologists contains articles on many of the points above.

Software and code

Policy information about availability of computer code

Data collection	Zeiss Zen for microscopy imaging.
Data analysis	Imaris v10.0.0 for image analysis.

For manuscripts utilizing custom algorithms or software that are central to the research but not yet described in published literature, software must be made available to editors and reviewers. We strongly encourage code deposition in a community repository (e.g. GitHub). See the Nature Research guidelines for submitting code & software for further information.

Data

Policy information about availability of data

All manuscripts must include a data availability statement. This statement should provide the following information, where applicable:

- Accession codes, unique identifiers, or web links for publicly available datasets
- A list of figures that have associated raw data
- A description of any restrictions on data availability

The main data discussed in this protocol are available in the supporting primary research papers (https://www.nature.com/articles/s43018-020-00147-8, https://www.nature.com/articles/s44161-022-00047-3, and https://www.cell.com/cell-metabolism/fulltext/S1550-4131(23)00010-4). The raw datasets of the main data and of the additional new data shown in this work are available for research purposes from the corresponding authors upon reasonable request.

Field-specific reporting

Please select the one below that is the best fit for your research. If you are not sure, read the appropriate sections before making your selection.

◉ Life sciences ○ Behavioural & social sciences ○ Ecological, evolutionary & environmental sciences

Life sciences study design

All studies must disclose on these points even when the disclosure is negative.

Sample size	Not applicable, as this work describes a protocol. The sample size information of the original works that adopted the described protocol can be
Data exclusions	No data excluded.
Replication	Not applicable, as this work describes a protocol. For the original works that adopted the described protocol, technical replicates and
Randomization	Not applicable, as this work describes a protocol. For the original works that adopted the described protocol, all mice used were age- and gender-
Blinding	Not applicable, as this work describes a protocol.

Behavioural & social sciences study design

All studies must disclose on these points even when the disclosure is negative.

Study description	
Research sample	
Sampling strategy	
Data collection	
Timing	
Data exclusions	
Non-participation	
Randomization	

Ecological, evolutionary & environmental sciences study design

All studies must disclose on these points even when the disclosure is negative.

Study description	
Research sample	
Sampling strategy	
Data collection	
Timing and spatial scale	
Data exclusions	
Reproducibility	
Randomization	
Blinding	

Did the study involve field work? ○ Yes ○ No

Field work, collection and transport

Field conditions	
Location	
Access & import/export	
Disturbance	

Reporting for specific materials, systems and methods

We require information from authors about some types of materials, experimental systems and methods used in many studies. Here, indicate whether each material, system or method listed is relevant to your study. If you are not sure if a list item applies to your research, read the appropriate section before selecting a response.

Materials & experimental systems

n/a	Involved in the study
	Antibodies
	Eukaryotic cell lines
	Palaeontology and archaeology
	Animals and other organisms
	Human research participants
	Clinical data
	Dual use research of concern

Methods

n/a	Involved in the study
	ChIP-seq
	Flow cytometry
	MRI-based neuroimaging

Antibodies

Antibodies used: The information of all used antibodies was included in the Methods, including manufacturers and catalog numbers.

Validation: All antibodies were purchased from commercial sources and have been validated by the vendors.

Eukaryotic cell lines

Policy information about cell lines

Cell line source(s):

Authentication:

Mycoplasma contamination:

Commonly misidentified lines (See ICLAC register):

Palaeontology and Archaeology

Specimen provenance:

Specimen deposition:

Dating methods:

☐ Tick this box to confirm that the raw and calibrated dates are available in the paper or in Supplementary Information.

Ethics oversight:

Note that full information on the approval of the study protocol must also be provided in the manuscript.

Animals and other organisms

Policy information about studies involving animals; ARRIVE guidelines recommended for reporting animal research

Laboratory animals: All animals were housed at room temperature with a 12-light/12-dark cycle in the Association for the Assessment and Accreditation of

Wild animals: The study did not involve wild animals.

Field-collected samples: The study did not involve samples collected from the field.

Ethics oversight: All experiments with mice were performed in accordance with a protocol approved by the Institutional Animal Care and Use Committee

Note that full information on the approval of the study protocol must also be provided in the manuscript.

Human research participants

Policy information about studies involving human research participants

Population characteristics: Healthy adult human volunteer donors with ages 18 to 65 and with all genders, races, and ethnicities.

Recruitment: Primary human monocytes were harvested and provided by Human Immunology Core at the University of Pennsylvania.

Ethics oversight: All specimens were collected under a University of Pennsylvania Institutional Review Board-approved protocol and written

Note that full information on the approval of the study protocol must also be provided in the manuscript.

Clinical data

Policy information about clinical studies

All manuscripts should comply with the ICMJE guidelines for publication of clinical research and a completed CONSORT checklist must be included with all submissions.

Clinical trial registration

Study protocol

Data collection

Outcomes

Dual use research of concern

Policy information about dual use research of concern

Hazards

Could the accidental, deliberate or reckless misuse of agents or technologies generated in the work, or the application of information presented in the manuscript, pose a threat to:

No	Yes	
○	○	Public health
○	○	National security
○	○	Crops and/or livestock
○	○	Ecosystems
○	○	Any other significant area

Experiments of concern

Does the work involve any of these experiments of concern:

No	Yes	
○	○	Demonstrate how to render a vaccine ineffective
○	○	Confer resistance to therapeutically useful antibiotics or antiviral agents
○	○	Enhance the virulence of a pathogen or render a nonpathogen virulent
○	○	Increase transmissibility of a pathogen
○	○	Alter the host range of a pathogen
○	○	Enable evasion of diagnostic/detection modalities
○	○	Enable the weaponization of a biological agent or toxin
○	○	Any other potentially harmful combination of experiments and agents

ChIP-seq

Data deposition

☑ Confirm that both raw and final processed data have been deposited in a public database such as GEO.

☑ Confirm that you have deposited or provided access to graph files (e.g. BED files) for the called peaks.

Data access links
May remain private before publication
GSE221949

Files in database submission

Genome browser session
(e.g. UCSC)

Methodology

Replicates

Sequencing depth

Antibodies

Peak calling parameters

Data quality

Software

Flow Cytometry

Plots

Confirm that:

☑ The axis labels state the marker and fluorochrome used (e.g. CD4-FITC).

☑ The axis scales are clearly visible. Include numbers along axes only for bottom left plot of group (a 'group' is an analysis of identical markers).

☑ All plots are contour plots with outliers or pseudocolor plots.

☑ A numerical value for number of cells or percentage (with statistics) is provided.

Methodology

Sample preparation	Tumors were isolated and subjected to mechanical dissociation with a gentleMACS Dissociator (Miltenyi) and enzymatic
Instrument	FACSCanto II flow cytometer (BD Biosciences)
Software	FlowJo software (Version 10.4)
Cell population abundance	More than 200 thousand cells were sorted.
Gating strategy	All cells were gated.

☑ Tick this box to confirm that a figure exemplifying the gating strategy is provided in the Supplementary Information.

Magnetic resonance imaging

Experimental design

Design type	
Design specifications	
Behavioral performance measures	

Acquisition

Imaging type(s)	
Field strength	
Sequence & imaging parameters	
Area of acquisition	

Diffusion MRI ○ Used ○ Not used

Preprocessing

Preprocessing software	
Normalization	
Normalization template	
Noise and artifact removal	
Volume censoring	

Statistical modeling & inference

Model type and settings	
Effect(s) tested	

Specify type of analysis: ○ Whole brain ○ ROI-based ○ Both

Statistic type for inference (See Eklund et al. 2016)	
Correction	

Models & analysis

n/a | Involved in the study

- ○ Functional and/or effective connectivity
- ○ Graph analysis
- ○ Multivariate modeling or predictive analysis

Functional and/or effective connectivity	
Graph analysis	
Multivariate modeling and predictive analysis	